UNIVERSITY OF CALIFORNIA, SAN DIEGO

The Regulation of Epithelial-Mesenchymal Transition by the Ubiquitin-Proteasome System

A dissertation submitted in partial satisfaction of the requirements
for the degree Doctor of Philosophy

in

Biomedical Sciences

by

Daniel Abraham Garcia

Committee in charge:

Professor John T. Chang, Chair
Professor Eric J. Bennett
Professor Gen-Sheng Feng
Professor Dwayne G. Stupack
Professor Jing Yang

2018

The Dissertation of Daniel Abraham Garcia is approved, and it is acceptable in quality and form for publication on microfilm and electronically:

Chair

University of California, San Diego

2018

DEDICATION

I dedicate this dissertation to all underrepresented people in the sciences – those who paved the way for me, those with whom I made this journey, and those who have yet to embark.

EPIGRAPH

I seem to have been only like a boy playing on the seashore, and diverting myself in now and then finding a smoother pebble or a prettier shell than ordinary, whilst the great ocean of truth lay all undiscovered before me.

Isaac Newton

TABLE OF CONTENTS

LIST OF ABBREVIATIONS

7-AAD	7-aminoacintomycin D
ABP	activity-based probe
ANOVA	analysis of variance
ARRIVE	Animal Research: Reporting of In Vivo Experiments
cDNA	complementary DNA
CSC	cancer stem cell
DAPI	4',6-diamidino-2-phenylindol
DMSO	dimethyl sulfoxide
DTT	dithiothreitol
DUB	deubiquitinase
EMT	epithelial-mesenchymal transition
FACS	fluorescence activated cell sorting
FBS	fetal bovine serum
FDR	false discovery rate
GEO	Gene expression omnibus
GFP	green fluorescent protein
GSEA	Gene set enrichment analysis
H&E	hematoxylin & eosin
HMLE	Immortalized human mammary epithelial cells
IPA	Ingenuity Pathway Analysis
MEGM	mammary epithelial growth medium
MFI	median fluorescence intensity

mut	mutant
NES	normalized enrichment score
NSG	NOD SCID gamma
PBS	phosphate buffered saline
qPCR, qRT-PCR	Quantitative real-time PCR
SDS-PAGE	Sodium dodecyl sulfate - polyacrylamide gel electrophoresis
SEM	Standard error of the mean
shRNA	short hairpin RNA
SSC	Side scatter
TCGA	The Cancer Genome Atlas
TGF-β	transforming growth factor-beta
wt	wild type

LIST OF FIGURES

ACKNOWLEDGEMENTS

I would like to thank my thesis advisor, John Chang, for reaching out to me and giving me the opportunity to join the Chang Lab as a graduate student. It has been a pleasure to have worked in such a collaborative and positive lab environment, and I am immensely thankful for John's full support in my development as an independent scientist.

Many talented individuals contributed to the completion of this dissertation work. I would like to acknowledge former and current members of the Chang Lab: Asoka Banno for starting the Proteasome-EMT project and giving me the opportunity to contribute and assume responsibility for the project; Eric van Baarsel, Pat Metz, Stella Widjaja, and Justine Lopez for their work and helpful discourse on the work presented in Chapters 1-2; Christina Baek and Tiffani Tysl for their contributions to the work presented in Chapter 4; Jane Klann for her flow cytometry expertise and helpful feedback during lab meeting presentations; Janilyn Arsenio, Brigid Boland, and Soo Ngoi for their critical feedback on experiments and manuscripts; Jocelyn Olvera, Lauren Quezada, Jad Kanbar, Nadia Kurd, Matt Tsai, and Max Mamroth for being awesome, friendly, and supportive lab members. Thank you to the entire Chang Lab for always being helpful, accommodating, and available when I needed assistance. I am glad to call myself a member of the Chang Gang.

I would like to acknowledge collaborators who have also contributed to this dissertation work: Jai Ablack from the Ginsberg Lab – you have been a source of molecular biology knowledge and career advice throughout my time as a graduate student; Maryan Rizk for sharing the luciferase constructs and expertise in the luciferase assay; Jing Yang, Eric Bennett, Paul Geurink, Bogdan Florea, Huib Ovaa, and Hermen Overkleeft for providing critical materials for

the studies; M. Valeria Estrada for the histologic analysis of lung tissue; members of the Bui Lab for sharing reagents and insightful discussions; neighboring labs (Ginsberg Lab, Eckmann Lab, Winzeler Lab, Rivera Lab, Nizet Lab, Haddad Lab, Nigam Lab) for sharing equipment and reagents.

I would like to acknowledge my thesis committee: Jing Yang, Eric J. Bennett, Dwayne G. Stupack, and Gen-Sheng Feng for their invaluable feedback, insight, guidance, and support. I chose you to be on my committee because I got the chance to know you through interactions during rotations and classes, and have great respect for you as scientists. Sharing my work with you all has been a great experience and has helped me develop into a better scientist. I greatly appreciate the time you spent in my committee meetings and reading my proposals and manuscripts.

The most important person I would like to thank is my partner in life, Elisa E. Villarreal. Elisa, your unconditional love and support has been essential to my success as a graduate student. Despite abnormal working hours, shifting deadlines, and many levels of uncertainty, you have managed to be an unwavering constant in my life – a constant source of encouragement, advice, compassion, and understanding. I also give Elisa credit for inspiring my exploration into science communication and outreach – an experience that has transformed me into a more engaged scientist.

Lastly, I would like to acknowledge my family: to my parents, Maggie and Abe, for instilling in me the importance of education and a curiosity for discovery that has flourished into my pursuit of a career in the sciences; to my siblings, David and Sofia, for being appreciative and supportive of my scientific endeavors, and for always making me laugh; to my grandparents,

Maria, Manuel, and Rachel, to whom I am indebted, for risking their livelihood and immigrating to the United States. Without their courage, I would not be here today.

Chapter 1-2, in full, are adapted versions of material published in *Oncotarget*. Banno, Asoka; Garcia, Daniel A.; van Baarsel, Eric D.; Metz, Patrick J.; Fisch, Kathleen; Widjaja, Christella E.; Kim, Stephanie H.; Lopez, Justine; Chang, Aaron N.; Geurink, Paul P.; Florea, Bogdan I.; Overkleeft, Hermen S.; Ovaa, Huib; Bui, Jack D.; Yang, Jing; Chang, John T.; Downregulation of 26S proteasome catalytic activity promotes epithelial-mesenchymal transition, *Oncotarget*, 2016, 7:21527-21541. The dissertation author was the co-primary author of all material.

Chapters 3-4, in full, are adapted versions of material that has been submitted for publication in *Molecular Cancer Research* and is under review. Garcia, Daniel A.; Baek, Christina; Estrada, M. Valeria; Tysl, Tiffani; Bennett, Eric J.; Yang, Jing; Chang, John T.; *Molecular Cancer Research*, In review. The dissertation author was the primary author of all material.

VITA

2010	B.S., Biology, Harvey Mudd College
2010-2012	Post-Baccalaureate Fellow, NIH, Bethesda, MD
2012-2017	Howard Hughes Medical Institute Gilliam Fellow
2018	Ph.D., Biomedical Sciences, University of California, San Diego

PUBLICATIONS

Van Dyken, Steven J; **Garcia, Daniel**; Porter, Paul; Huang, Xiaozhu; Quinlan, Patricia J; Blanc, Paul D; Corry, David B; Locksley, Richard M; Fungal chitin from asthma-associated home environments induces eosinophilic lung infiltration. *The Journal of Immunology*, **2011**, 187:2261-7.

Banno, Asoka*; **Garcia, Daniel A***; van Baarsel, Eric D; Metz, Patrick J; Fisch, Kathleen; Widjaja, Christella E; Kim, Stephanie H; Lopez, Justine; Chang, Aaron N; Geurink, Paul P; Florea, Bogdan I; Overkleeft, Hermen S; Ovaa, Huib; Bui, Jack D.; Yang, Jing; Chang, John T. *Oncotarget*, **2016**, 7:21527-21541. *co-primary authors

Widjaja, Christella E; Olvera, Jocelyn G; Metz, Patrick J; Phan, Anthony T; Savas, Jeffrey N; De Bruin, Gerjan; Leestemaker, Yves; Berkers, Celia R; De Jong, Annemieke; Florea, Bogdan I; Fisch, Kathleen; Lopez, Justine; Kim, Stephanie H; **Garcia, Daniel A**; Searles, Stephen; Bui, Jack D; Chang, Aaron N; Yates III, John R; Goldrath, Ananda W; Overkleeft, Hermen S; Ovaa, Huib; Chang, John T. *The Journal of Clinical Investigation*, **2017**, 127:3609-3623.

Garcia, Daniel A; Baek, Christina; Estrada, M Valeria; Tysl, Tiffani; Bennett, Eric J; Yang, Jing; Chang, John T. Ubiquitin specific peptidase 11 (USP11) enhances TGF-β-induced epithelial-mesenchymal plasticity and human breast cancer metastasis. In review.

ABSTRACT OF THE DISSERTATION

The Regulation of Epithelial-Mesenchymal Transition by the Ubiquitin-Proteasome System

by

Daniel Abraham Garcia

Doctor of Philosophy in Biomedical Sciences

University of California, San Diego, 2018

Professor John T. Chang, Chair

Epithelial-mesenchymal transition (EMT) is a conserved cellular plasticity program that is reactivated in carcinoma cells and drives metastasis. EMT is well studied, but its regulatory mechanisms remain unclear. In this dissertation, I explore two ways in which the ubiquitin-proteasome system regulates EMT.

First, I investigate the role of the 26S proteasome in regulating EMT. In Chapters 1-2, I show that β2 and β5 proteasome subunit activity is downregulated during EMT in immortalized human mammary epithelial cells. Moreover, selective proteasome inhibition enabled mammary epithelial cells to acquire certain morphologic and functional characteristics reminiscent of cancer stem cells, including CD44 expression, self-renewal, and tumor formation. Transcriptomic analyses suggested that proteasome-inhibited cells share gene expression signatures with cells that have undergone EMT, in part, through modulation of the TGF-β signaling pathway. These findings suggest that selective downregulation of proteasome activity in mammary epithelial cells can initiate the EMT program and acquisition of a cancer stem cell-like phenotype. As proteasome inhibitors become increasingly used in cancer treatment, my findings highlight a potential risk of these therapeutic strategies and suggest a possible mechanism by which carcinoma cells may escape from proteasome inhibitor-based therapy.

Second, I explore potential novel regulators of EMT within the ubiquitin-proteasome system pathway. In Chapters 3-4, I uncover novel regulators of EMT by mining previously published microarray data and found a group of deubiquitinases (DUBs) upregulated in cells that have undergone EMT. Here, I show that one DUB in particular, Ubiquitin specific peptidase 11 (USP11), enhances TGF-β-induced EMT and self-renewal in immortalized human mammary epithelial cells. Furthermore, modulating USP11 expression in human breast cancer cell lines altered migratory capacity in vitro and metastasis in vivo. Moreover, I found that high USP11 expression in human breast cancer patient clinical samples correlated with decreased survival. Mechanistically, modulating USP11 expression altered the stability of TGF-β receptor type 2 (TGFBR2) and TGF-β downstream signaling in human breast cancer cell lines. Together, these data suggest that deubiquitination of TGFBR2 by USP11, effectively spares TGFBR2 from

proteasomal degradation to promote EMT and metastasis and suggest USP11 as a potential therapeutic target for breast cancer.

INTRODUCTION

Cancer is one of the leading causes of death in the United States, and up to 90% of cancer-associated mortality can be attributed to therapy-resistant metastatic disease (1). Despite intense investigation, metastasis continues to be a poorly understood aspect of cancer progression (2). While deaths due to metastasis are likely to be abrogated by increased efforts in early detection of cancer, there is a need for more effective metastasis-specific therapies in the clinic (3).

Metastasis is fueled by disseminating tumor cells following a complex cascade of events starting with translocation of primary tumor cells to a distant site and culminating with the development into a lethal outgrowth in distant organs. During the metastatic cascade, tumor cells gain the capacity to invade locally and disseminate into the vasculature. However, not all cells that enter the vasculature go on to colonize distant sites. Only a small subset of invading tumor cells acquire characteristics of cancer stem cells (CSCs) needed to establish macrometastases, namely self-renewal capacity, proliferative potential, and chemoresistance (2). There is increasing evidence to support the involvement of CSCs in multiple types of hematologic and solid tumors, including breast, brain, prostate, colon, liver, and pancreatic, among others (4). Although the ontogeny of CSCs is incompletely understood, a developmental process known as the epithelial-mesenchymal transition (EMT) has been shown to promote the development of cells with CSC properties (5-9). Previous studies have identified the transcription factors TWIST1, SNAI1, and ZEB1 as key inducers of EMT, metastasis, and the CSC phenotype (4,7,9-11). Thus, identifying the factors that regulate EMT is highly relevant to cancer therapy as these stimuli can be targeted to block metastasis, and potentially CSC formation, in carcinomas.

Recent evidence suggests that CSCs may exhibit decreased proteasome activity (12-16). The 26S proteasome is comprised of a 20S core complex that contains β1, β2, and β5 catalytic subunits that contain caspase-like, trypsin-like, and chymotrypsin-like proteolytic sites, respectively (17,18). The observation of decreased proteasome activity in CSCs led us to hypothesize that downregulation of proteasome activity might be causally related to the acquisition of the CSC phenotype, via EMT. This question will be addressed in Chapters 1-2.

Another well-studied driver of metastasis is microenvironment-derived transforming growth factor-β (TGF-β). TGF-β is a cytokine that is known to promote cancer metastasis through multiple mechanisms, including enhancing invasive properties, stemness, and permissive effects on the tumor microenvironment (19,20). Interestingly, TGF-β is a potent inducer of EMT; thus, metastasis relies, in part, on TGF-β's ability to induce an EMT program (21). The link between TGF-β and EMT is mechanistically clear: upon TGF-β type I and type II receptor (TGFBR1 and TGFBR2) heterocomplex activation by the ligand TGF-β1, SMAD2/3 are phosphorylated and shuttled to the nucleus with SMAD4 to regulate expression of EMT transcription factors (11). However, what remain unclear are the ubiquitin-proteasome regulatory mechanisms of TGF-β signaling in the context of EMT and metastasis. Importantly, a deeper understanding of this mode of regulation may reveal novel enzymes that can be subject to rational and specific drug design.

There is increasing support for the importance of the ubiquitin-proteasome system in regulating EMT and cancer progression. Low proteasome activity is associated with the cancer stem cell state and EMT, and treatment of epithelial cells with proteasome inhibitors can induce EMT (22,23). In addition, a number of deubiquitinases (DUBs) have been implicated in cancer progression and metastasis, such as DUB3, USP4, USP13, USP15, USP28, and USP51 (24-29).

Based on this work and the context-specific nature of EMT, I hypothesize that there exists a set of proteins within the ubiquitin-proteasome pathway that regulate EMT specifically in normal and neoplastic human mammary epithelial cells. These questions will be addressed in Chapters 3-4.

CHAPTER 1: PROTEASOME ACTIVITY REGULATES EPITHELIAL-MESENCHYMAL TRANSITION

1.1: Introduction

I first sought to determine whether cells undergoing EMT alter their levels of proteasome activity. I utilized immortalized human mammary epithelial (HMLE) cells in which EMT can be induced by stable overexpression of *SNAI1* or *TWIST1*, or by treatment with TGF-β1 (hereafter referred to as HMLE-Snail, HMLE-Twist, or HMLE+TGF-β1, respectively), as previously described (7,30-33). In this model system, the HMLE cell line was created by immortalizing primary epithelial cells – isolated from a human reduction mammoplasty – with hTERT at SV40 large T antigen. HMLE cells have epithelial morphology, express epithelial markers E-cadherin and cytokeratins 14 and 18, and lack expression of mesenchymal markers (34). When EMT is induced in HMLE cells by ectopic expression of *SNAI1* or *TWIST1* or treatment with TGF-β1, the resulting cells acquire mesenchymal characteristics – both in terms of morphology and mRNA marker expression (7). Notably, HMLE cells that have undergone EMT exhibit characteristic cell surface expression phenotype of $CD44^{high}$, the same phenotype observed in neoplastic mammary stem cells (7). Here, I use HMLE cells as a robust model system to study EMT and its regulatory mechanisms.

1.2: Results

1.2.1: Downregulation of proteasome activity is associated with EMT

I determined proteasome activity by using subunit-specific probes that bind irreversibly to the β1, β2, or β5 proteasome catalytic subunits (**Fig. 1.1**) (35-37). I observed that cells that had undergone EMT exhibited a 25-30% reduction in β2 and β5, but not β1, subunit activity compared to cells that had not undergone EMT (**Fig. 1.2**). This is likely due to a reduction in specific proteasome activity, since total protein and mRNA expression of these subunits

remained unaffected by EMT induction (**Fig. 1.3**). In support of this finding, I observed that cells that had undergone EMT also exhibited an accumulation of ubiquitinated proteins, compared to their epithelial parental cells (**Fig. 1.2**). Taken together, these data suggest that HMLE cells decrease specific proteasome catalytic activities – not proteasome amounts – during EMT.

1.2.2: Low proteasome activity is associated with human breast cancer and decreased patient survival

To determine whether the link between reduced proteasome activity and tumorigenicity might apply to human patients with breast carcinoma, I analyzed publicly available gene expression data from the Oncomine Platform and The Cancer Genome Atlas. Intriguingly, I found that tumor samples from patients with invasive breast carcinoma exhibited significantly lower *PSMB2* and *PSMB5* proteasome subunit mRNA expression compared to samples derived from normal tissue (**Fig. 1.4**). Moreover, breast cancer patients with tumors exhibiting the lowest quartile of *PSMB2* and *PSMB5* combined mRNA expression showed reduced 5-year survival compared to patients with tumors in the highest quartile (**Fig. 1.4**). Together, these data suggest that low proteasome subunit expression may be useful as an indicator of poor prognosis for breast cancer patients.

1.2.3: Selective inhibition of proteasome activity induces the EMT phenotype

To investigate whether the reduction in proteasome activity is mechanistically linked to the process of EMT, I treated HMLE cells with selective β1, β2, or β5 proteasome subunit inhibitors (**Fig. 1.1**) (37-39). I then assessed the cell surface expression of CD44 by HMLE cells after 14 days of treatment. High expression of CD44 has been associated with human breast cancer stem cells as well as with HMLE cells that have undergone EMT (7,40,41). Strikingly, 98% of cells treated with β2 subunit inhibitor and 57% of those treated with β5 subunit inhibitor

expressed high levels of CD44, compared to 12% of DMSO-treated cells (**Fig. 1.5**). By contrast, cells treated with the β1 subunit inhibitor expressed low levels of CD44 (**Fig. 1.5**) consistent with the lack of change in β1 subunit proteasome activity within cells that had undergone EMT (**Fig. 1.2**). To exclude the possibility that the increase of the $CD44^{high}$ population was due to selective outgrowth of $CD44^{high}$ cells, HMLE cells were first FACS sort-purified for low expression of CD44, then treated with selective proteasome inhibitors (**Fig. 1.6**). I found that $CD44^{low}$ cells treated with proteasome inhibitors gave rise to $CD44^{high}$ cells after 14 days of treatment, demonstrating that these cells arose directly from $CD44^{low}$ cells (**Fig. 1.6**).

$CD44^{high}$ cells that emerged after treatment with selective β2 or β5 subunit inhibitors lost their cobblestone-like appearance and acquired the fibroblast-like morphology characteristic of mesenchymal cells (**Fig. 1.5**). Moreover, cells treated with selective proteasome inhibitors decreased their expression of epithelial marker E-cadherin and increased their expression of mesenchymal markers fibronectin and vimentin, as shown by immunofluorescence and immunoblot analyses (**Fig. 1.5**). Together, these results suggest that selective β2 or β5 subunit inhibition induces HMLE cells to acquire an EMT phenotype.

In addition to exhibiting mesenchymal characteristics, I found that cells with lower levels of proteasome activity exhibited decreased apoptosis, in comparison to parental HMLE cells, when treated with the pan-proteasome inhibitor epoxomicin (**Fig. 1.7**). These results suggest that the reduced level of proteasome activity associated with EMT confers increased resistance to the cytotoxic effects of pan-proteasome inhibition. Furthermore, these results are consistent with prior observations that CSCs may be more resistant to proteasome inhibitors (15).

I found that a second non-tumorigenic human mammary epithelial cell line, MCF10A, also downregulated β2 and β5 subunit activity while undergoing EMT in response to TGF-β1 (**Fig. 1.8**). MCF10A cells have been previously shown to decrease their expression of CD24 as they undergo EMT (8). I observed a decrease in CD24 expression in MCF10A cells treated with selective β2 or β5 subunit inhibitors, suggesting that these cells had undergone EMT (**Fig. 1.9**). In addition, MCF10A cells treated with β2 or β5 subunit inhibitors exhibited a fibroblast-like morphology, decreased expression of epithelial markers, and increased expression of mesenchymal markers at the protein and mRNA levels (**Fig. 1.9**). Together, these results suggest that induction of the EMT phenotype as a result of selective β2 or β5 inhibition of proteasome activity may be a generalizable phenomenon.

1.2.4: Cells treated with selective proteasome inhibitors acquire the ability to self-renew

I next sought to confirm that the $CD44^{high}$ cells that had arisen following treatment with proteasome inhibitors had indeed undergone EMT. I focused my studies on β2 subunit inhibition due to its more pronounced effect (**Fig. 1.5**). It has been previously demonstrated that HMLE cells that have undergone EMT exhibit an increased ability to self-renew, a characteristic typically associated with mammary epithelial stem cells (7,42,43). I therefore tested the ability of HMLE cells treated with proteasome inhibitors to form mammospheres, a capability indicative of self-renewal activity. Indeed, β2 subunit inhibitor-treated HMLE cells acquired an enhanced capacity to form mammospheres compared to DMSO-treated cells, both in primary assays and during subsequent serial passages (**Fig. 1.10**). These results suggest that selective proteasome inhibition confers self-renewal capabilities to HMLE cells.

1.2.5: Selective inhibition of proteasome activity endows HMLER cells with tumor-initiating capacity in vivo

I next wished to determine whether selective proteasome inhibition also endowed HMLE cells with the ability to initiate tumors, another property of CSCs. Accordingly, I used a tumor xenograft system in which HMLE cells constitutively expressing *RAS-V12H* oncogene and *TWIST1* (HMLER-Twist) renders them tumorigenic when injected into immunodeficient mice (34). Similar to the behavior of proteasome-inhibited HMLE cells described above, HMLER cells treated with β2 subunit inhibitor acquired a $CD44^{high}$ phenotype and the ability to form mammospheres (**Fig. 1.11**). To test the tumorigenic potential of these cells, I injected HMLER, HMLER-Twist, or β2 subunit inhibitor-treated HMLER cells into immunodeficient mice. 92% of mice injected with HMLER-Twist or β2 inhibitor-treated HMLER cells developed tumors with a mean size of 0.5 cm; in contrast, mice injected with DMSO-treated HMLER cells did not develop tumors (**Fig. 1.11**). Taken together, these results suggest that downregulation of proteasome activity in HMLER cells can induce EMT and confer self-renewal and tumor-initiating capabilities, which are hallmarks of CSCs.

1.3: Conclusion

In this study, using HMLE cells – a robust EMT model – has allowed us to show the importance of 26S proteasome catalytic activity during EMT. I found that epithelial cells decrease their proteasome activity during EMT, in the setting of both ectopic expression of EMT transcription factors (TWIST and SNAI1) and treatment with TGF-β. Strikingly, I observed that selective inhibition of β2 or β5 subunit proteasome activity was sufficient to induce HMLE and MCF10A cells to acquire key morphologic and functional characteristics of the EMT, in terms of morphology, expression of markers at the mRNA and protein level, antigenic phenotype (CD44 cell surface expression), and functional assays (mammosphere and tumorigenesis assays). I also show a correlation between decreased expression of proteasome catalytic subunits and decreased

survival in a cohort of breast cancer patients. Taken together, these data suggest that downregulation of proteasome activity in breast cancer cells can initiate the EMT program, thereby conferring upon these cells key attributes of CSCs. These results further suggest that 26S proteasome catalytic activity is a novel regulator of EMT and could influence cancer disease progression in humans. The manner by which decreased proteasome activity induces EMT is still an open question and is addressed in Chapter 2.

Chapter 1, in full, is an adapted version of material published in *Oncotarget*. Banno, Asoka; Garcia, Daniel A.; van Baarsel, Eric D.; Metz, Patrick J.; Fisch, Kathleen; Widjaja, Christella E.; Kim, Stephanie H.; Lopez, Justine; Chang, Aaron N.; Geurink, Paul P.; Florea, Bogdan I.; Overkleeft, Hermen S.; Ovaa, Huib; Bui, Jack D.; Yang, Jing; Chang, John T.; Downregulation of 26S proteasome catalytic activity promotes epithelial-mesenchymal transition, *Oncotarget*, 2016, 7:21527-21541. The dissertation author was the co-primary author of all material.

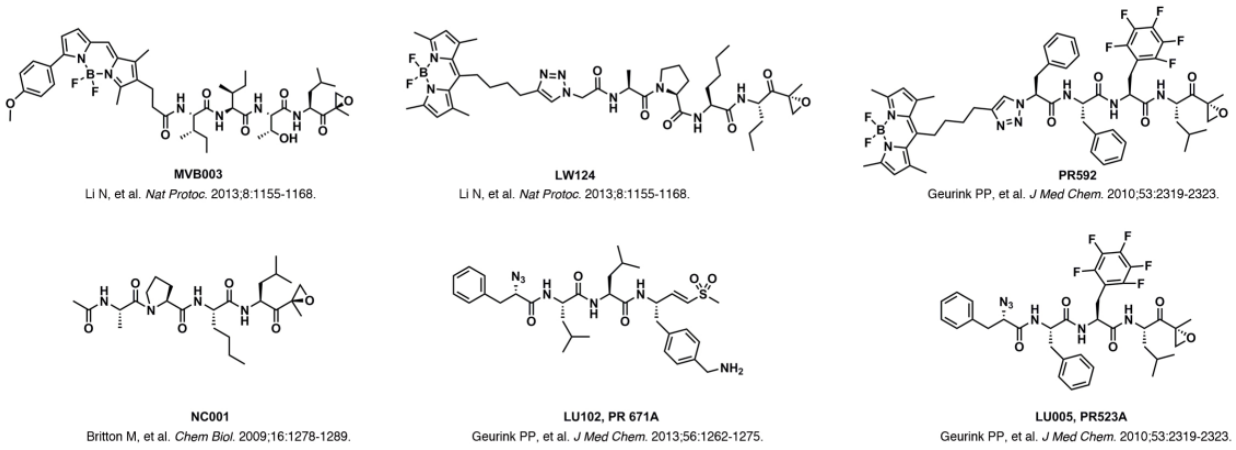

Figure 1.1. Structures of proteasome activity-based probes and selective proteasome inhibitors.

The pan-reactive (MVB003), β1 (LW124), β5 (PR592) subunit-specific probes, and β1 (NC001), β2 (LU102, PR671A), β5 (LU005, PR523A) subunit-specific inhibitors used in the study have been previously described (35-38).

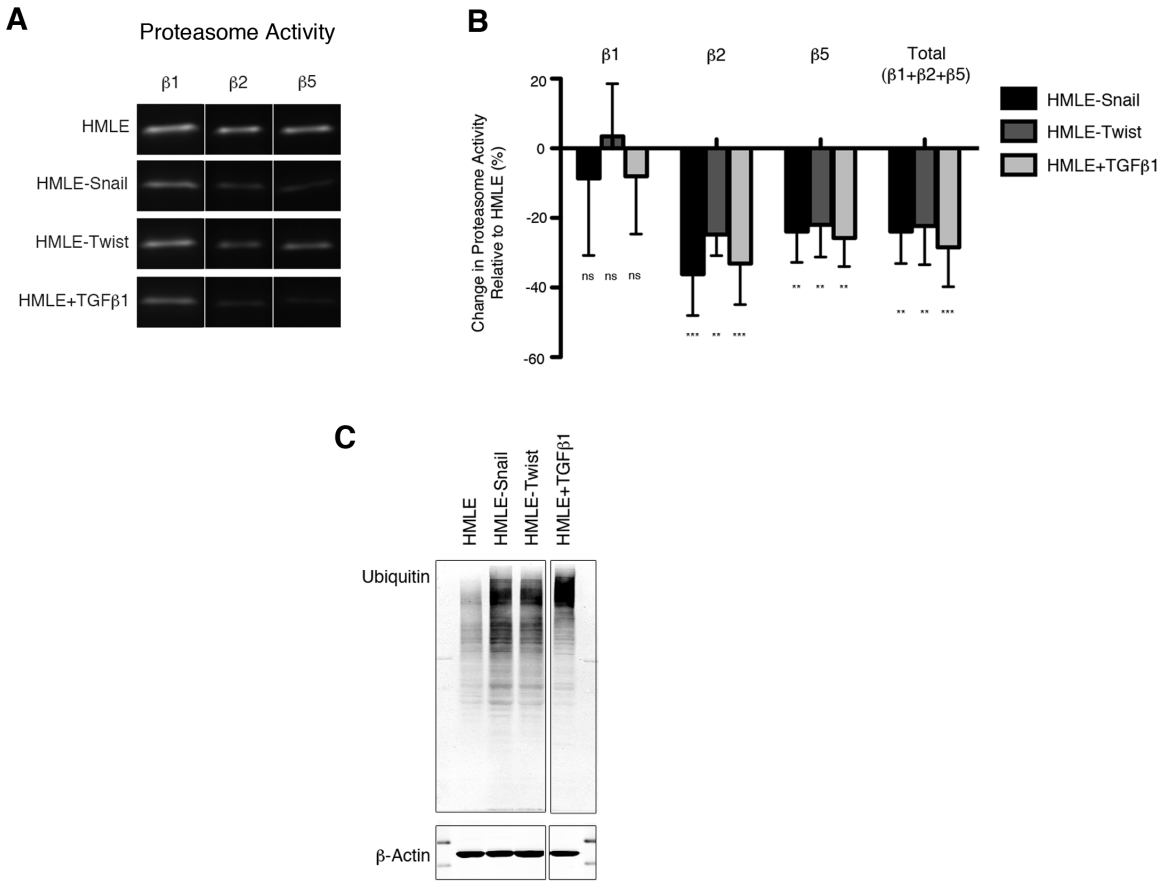

Figure 1.2. Downregulation of proteasome activity is associated with EMT.
(**A**) β1, β2, and β5 subunit proteasome activity in HMLE, HMLE-Snail, HMLE-Twist, and HMLE+TGF-β1 were measured by in-gel proteasome activity assay. Representative images of the SDS-PAGE gels are shown. Vertical spaces inserted between lanes indicate removal of intervening, irrelevant samples. All the samples were run on the same gel and imaged in a single scan. (**B**) Quantification of β1, β2, and β5 subunit activity as well as total catalytic activity (the sum of the three subunits) presented as percent change relative to HMLE. Error bars indicate standard error of the mean (SEM) ($n \geq 3$). (**C**) Immunoblot of whole cell lysates from HMLE cells using an anti-ubiquitin antibody, representative of 3 independent experiments. β-actin served as a loading control. Vertical spaces inserted between lanes indicate removal of intervening, irrelevant samples. All the samples were run on the same gel, transferred and blotted together, and imaged in a single scan.

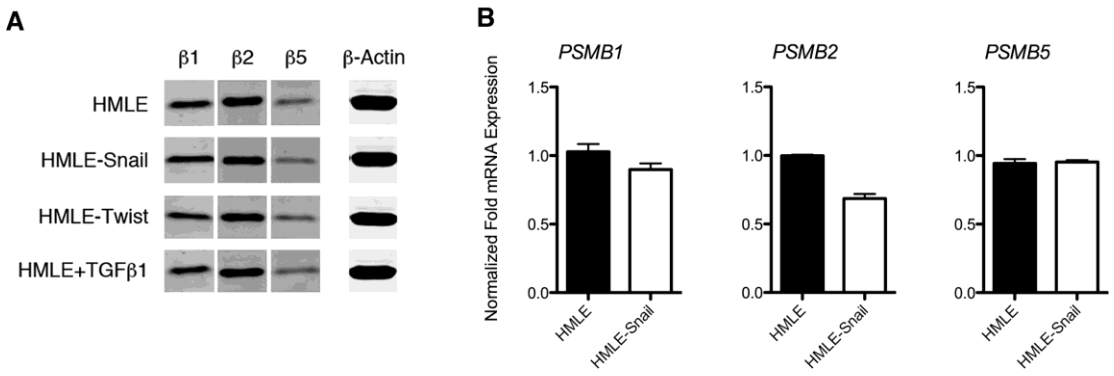

Figure 1.3. Proteasome subunit expression is unchanged during EMT.
(**A**) Total protein expression of the β1, β2, and β5 catalytic subunits was assessed by Western blotting with respective antibodies. A representative blot is shown. The blot was also probed for b-Actin, as a loading control. The vertical space inserted between lanes indicates where I removed intervening, irrelevant samples. (**B**) mRNA levels of HMLE parental cells and HMLE cells overexpressing Snail (HMLE-Snail). Data are shown as fold-change normalized to HMLE. Error bars indicate SEM (n = 3).

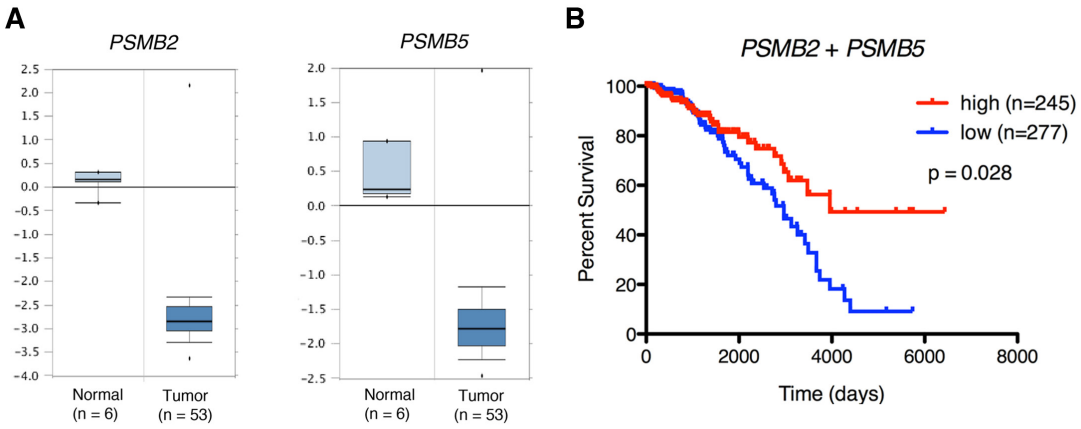

Figure 1.4. Low proteasome subunit expression is associated with breast tissue from patients with breast cancer and decreased patient survival.
(**A**) *PSMB2* and *PSMB5* gene expression box plots from normal and tumor samples from the Finak dataset (44). (**B**) Kaplan-Meier survival curves for breast cancer patients stratified by intra-tumor expression ("high" *vs* "low") of *PSMB2*and *PSMB5* mRNA.

Figure 1.5. Selective inhibition of proteasome activity induces an EMT phenotype.
(**A**) Flow cytometry analysis of CD44 surface expression and side scatter (SSC) after 14 days of treatment with DMSO or β1, β2, or β5 subunit inhibitor. Percentage of $CD44^{high}$ cells within the live population is indicated. Representative result of three independent experiments is shown. (**B**) Representative brightfield images of HMLE, HMLE+β2 inhibitor, HMLE+β5 inhibitor, and HMLE-Snail after 14 days of treatment. All the images were taken at 10X magnification. Schematic diagram depicts the change in cell morphology during EMT. (**C**) Confocal microscopy of E-cadherin (left panel; green), fibronectin (right panel; green), or vimentin (red) in HMLE cells treated with β2 subunit inhibitor or β5 subunit inhibitor for 14 days. Images were taken at 40X magnification. (**D**) Immunoblot of whole cell lysates from HMLE, HMLE+β2 inhibitor, HMLE+β5 inhibitor, or HMLE+TGF-β1 using anti-E-cadherin, anti-fibronectin, and anti-vimentin antibodies, representative of 3 independent experiments. β-actin served as a loading control.

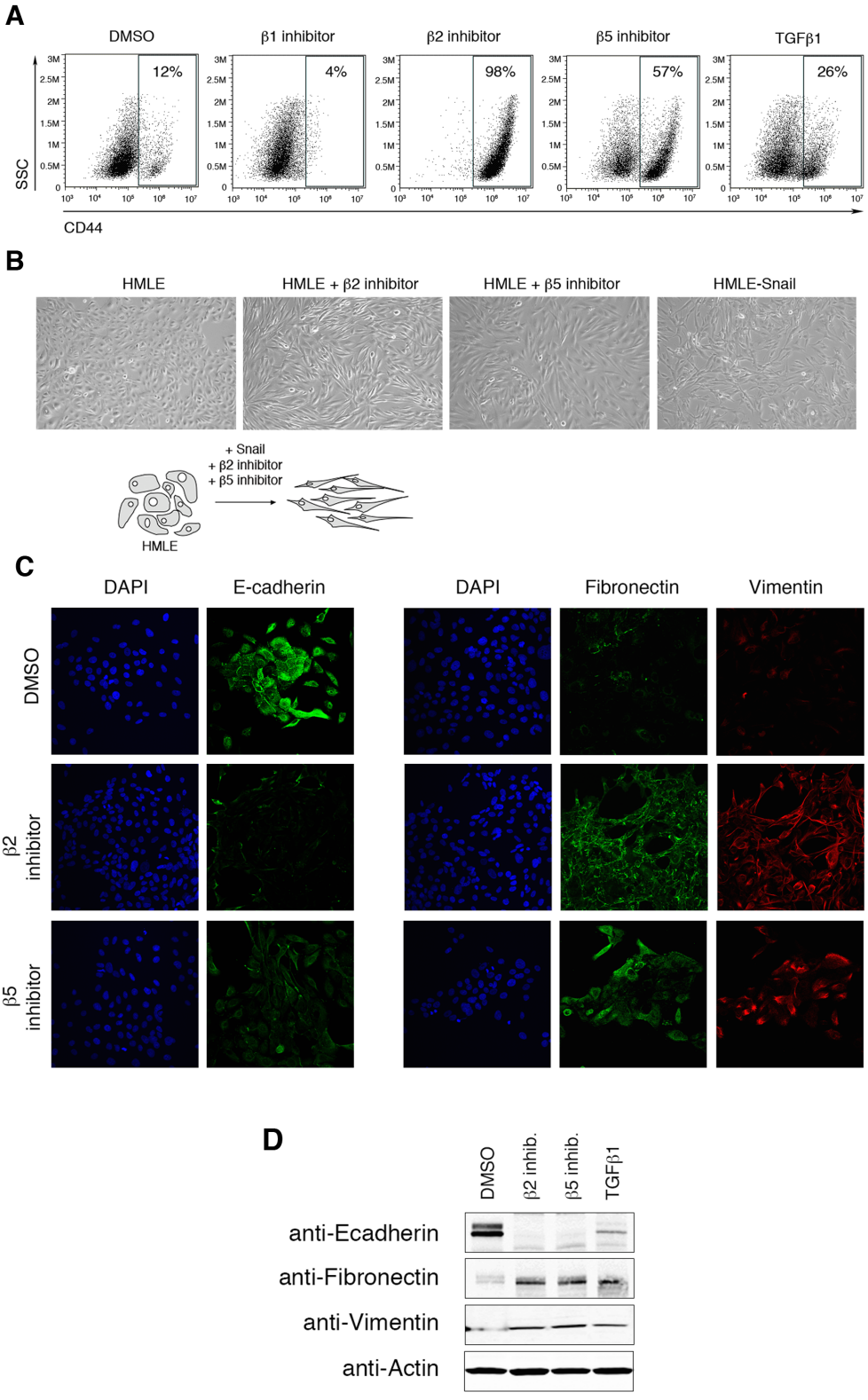
A
DMSO
β1 inhibitor
β2 inhibitor
β5 inhibitor
TGFβ1
12%
4%
98%
57%
26%
SSC
CD44
B
HMLE
HMLE + β2 inhibitor
HMLE + β5 inhibitor
HMLE-Snail
+ Snail
+ β2 inhibitor
+ β5 inhibitor
HMLE
C
DAPI
E-cadherin
DAPI
Fibronectin
Vimentin
DMSO
β2 inhibitor
β5 inhibitor
D
DMSO
β2 inhib.
β5 inhib.
TGFβ1
anti-Ecadherin
anti-Fibronectin
anti-Vimentin
anti-Actin

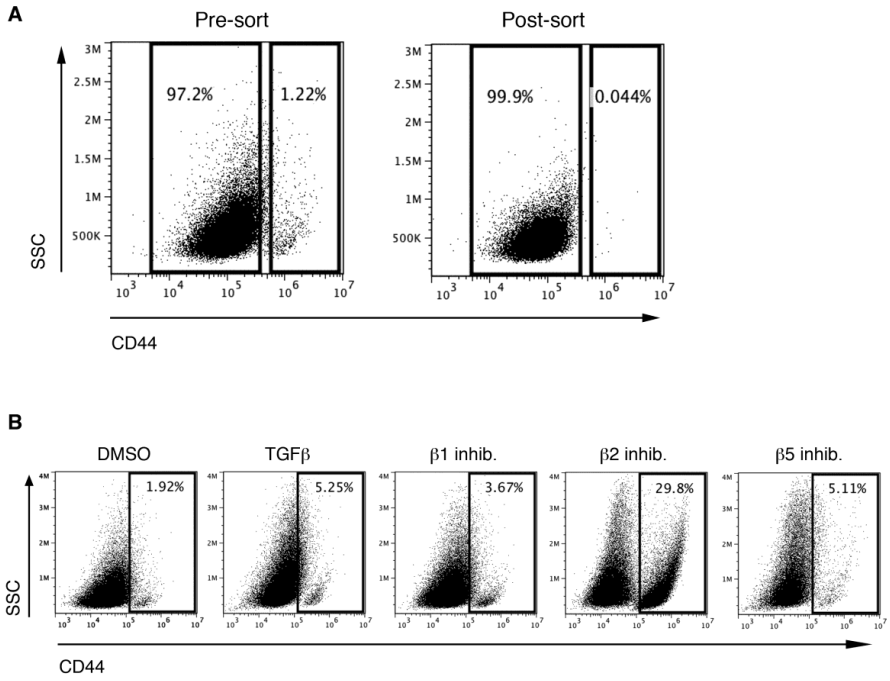

Figure 1.6. HMLE CD44^{high} cells arise from CD44^{low} cells during EMT or proteasome inhibitor treatment.

(**A**) Flow cytometry analysis of CD44 surface expression and side scatter (SSC) of HMLE parental cells before ("Pre-sort") and after ("Post-sort") sorting for low expression of CD44. Percentage of CD44^{low} cells (left gate) and CD44^{high} cells (right gate) within the live population is indicated. (**B**) Flow cytometry analysis of CD44 surface expression and side scatter (SSC) of HMLE CD44^{low} cells treated with DMSO, TGF-β, β1 inhibitor, β2 inhibitor, or β5 inhibitor for 14 days. Percentage of CD44^{high} cells within the live population is indicated.

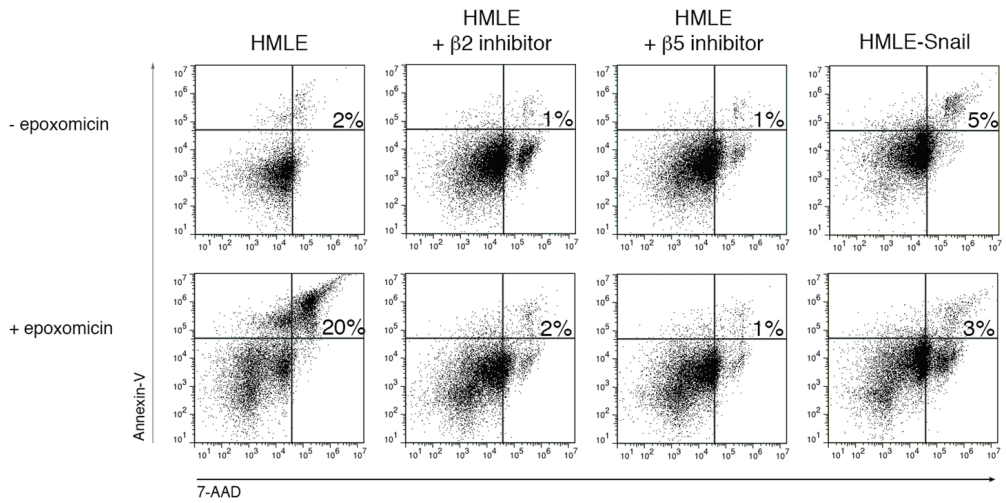

Figure 1.7. HMLE cells that have undergone EMT exhibit increased resistance to epoxomicin-induced apoptosis.

Flow cytometric analysis of 7-AAD and Annexin-V expression in HMLE, HMLE+β2 inhibitor, HMLE+β5 inhibitor, and HMLE-Snail with or without 1 day of epoxomicin treatment. Percentage of 7-AAD$^+$/Annexin V$^+$ cells is indicated. Representative result of three independent experiments is shown.

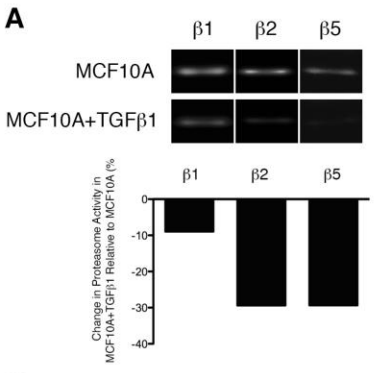

Figure 1.8. Downregulation of proteasome activity is associated with EMT in MCF10A cells.

β1, β2, and β5 subunit proteasome activity in MCF10A alone or treated with TGF-β1 was measured by in-gel proteasome activity assay. A representative SDS-PAGE gel is shown. Vertical spaces inserted between lanes indicate removal of intervening, irrelevant samples. All the samples were run on the same gel and imaged in a single scan. Quantification of β1, β2, and β5 subunit activity is presented as percent change relative to MCF10A.

Figure 1.9. Selective inhibition of proteasome activity induces an EMT phenotype in MCF10A cells.

(**A**) Flow cytometry analysis of CD24 surface expression in MCF10A after approximately 14 days of treatment with β2 subunit inhibitor, β5 subunit inhibitor, or TGF-β1 (open histograms) compared to DMSO treatment (grey-shaded histogram). (**B**) Representative brightfield images of MCF10A treated with DMSO or β2 inhibitor, β5 inhibitor, and TGF-β1 after 14 days of treatment. All the images were taken at 10X magnification. (**C**) Confocal microscopy of E-cadherin (left panel; green), Fibronectin (right panel; green), or Vimentin (red) in MCF10A cells treated with β2 subunit inhibitor or β5 subunit inhibitor. Images were taken at 40X magnification. (**D**) Immunoblot of whole cell lysates from MCF10A cells treated with DMSO, β2 inhibitor, β5 inhibitor, or TGF-β1 using anti-E-cadherin, and anti-Fibronectin antibodies, representative of 3 independent experiments. b-Actin served as a loading control. (**E**) mRNA levels of epithelial (*TJP1*, *SMURF1*, *SMURF2*, and *SMAD7*) and mesenchymal markers (*FN1*, *ZEB1*, *ZEB2*, *MMP2*, and *VIM*) in MCF10A+β2 inhibitor (black bars) or MCF10A+β5 inhibitor (grey bars). GAPDH was used as a reference gene. Data are shown as fold-change relative to DMSO-treated MCF10A. Error bars indicate SEM (n = 3).

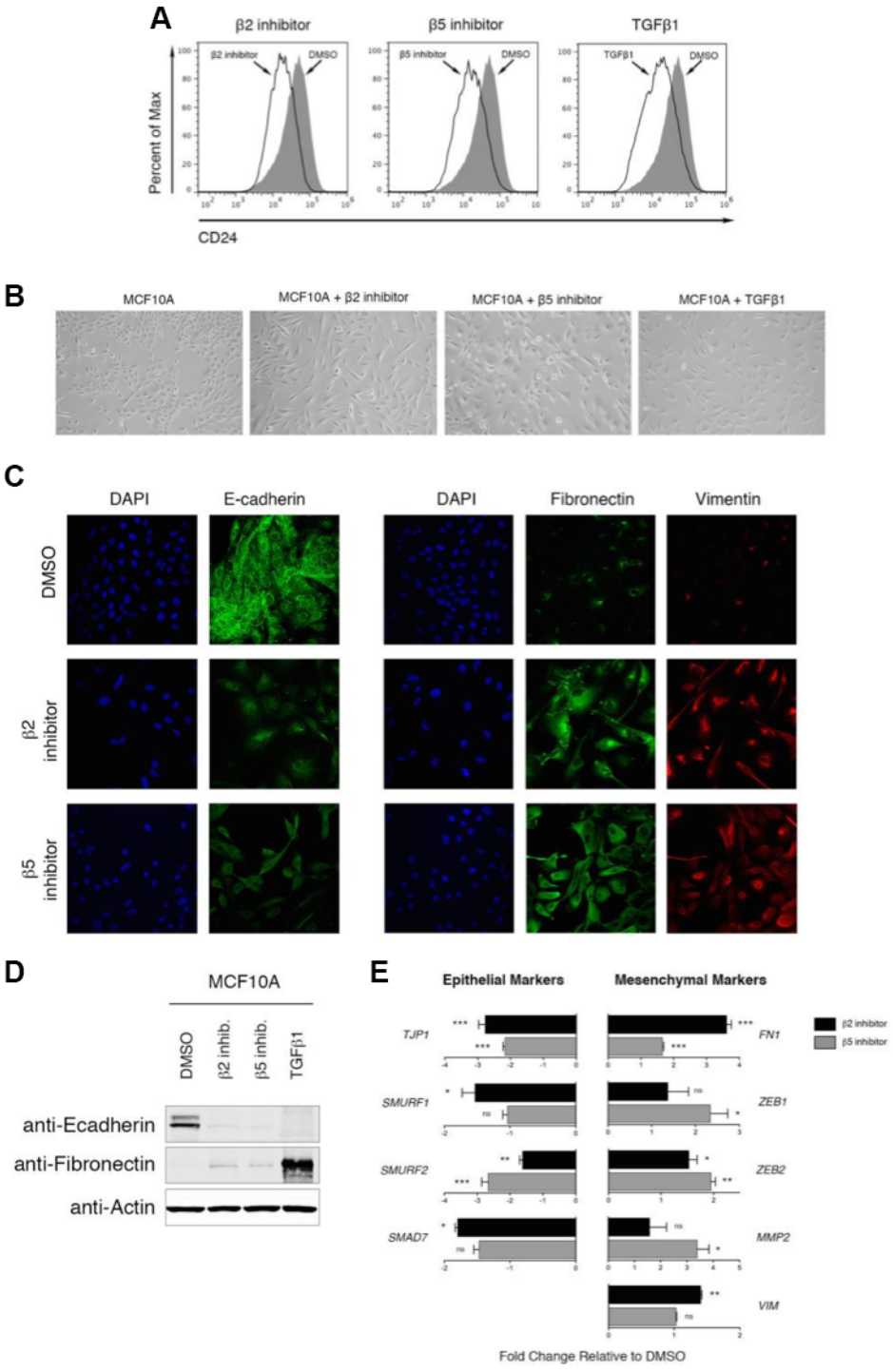
A
β2 inhibitor
β5 inhibitor
TGFβ1
DMSO
Percent of Max
CD24
B
MCF10A
MCF10A + β2 inhibitor
MCF10A + β5 inhibitor
MCF10A + TGFβ1
C
DAPI
E-cadherin
Fibronectin
Vimentin
DMSO
β2 inhibitor
β5 inhibitor
D
MCF10A
DMSO
β2 inhib.
β5 inhib.
TGFβ1
anti-Ecadherin
anti-Fibronectin
anti-Actin
E
Epithelial Markers
Mesenchymal Markers
TJP1
SMURF1
SMURF2
SMAD7
FN1
ZEB1
ZEB2
MMP2
VIM
Fold Change Relative to DMSO

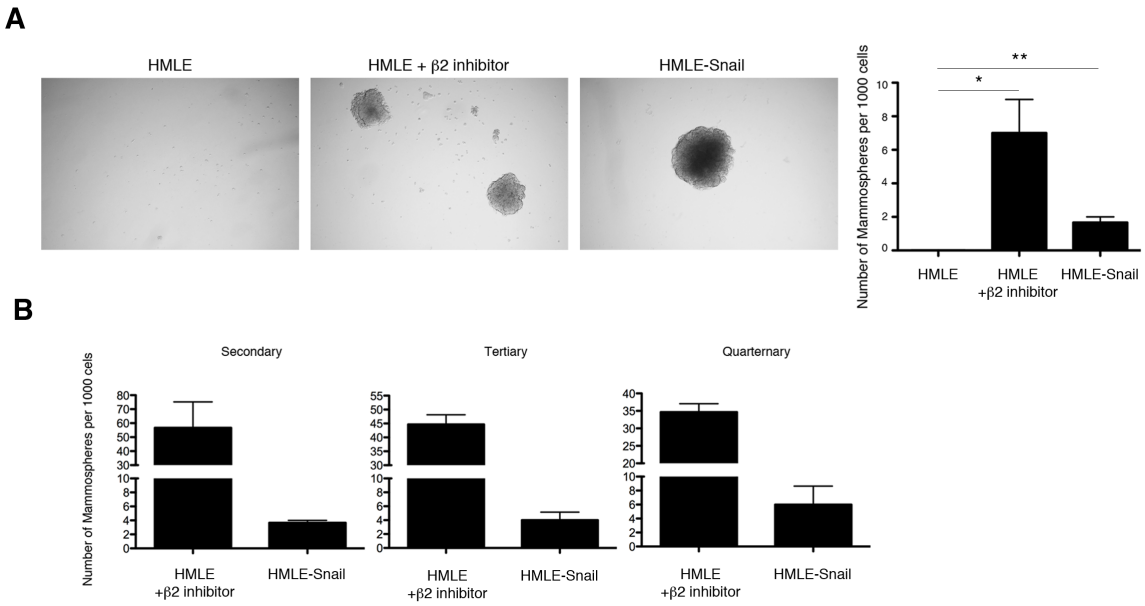

Figure 1.10. Selective inhibition of proteasome activity endows HMLE cells with self-renewal ability.

(A) Quantification of primary mammospheres per 1000 seeded cells formed by HMLE, HMLE+β2 inhibitor, or HMLE-Snail. Error bars indicate SEM ($n \geq 3$). **(B)** Serial passage of mammospheres. Quantification is presented in the bar graph as the number of mammospheres formed per 1000 seeded cells. Error bars indicate SEM ($n = 3$).

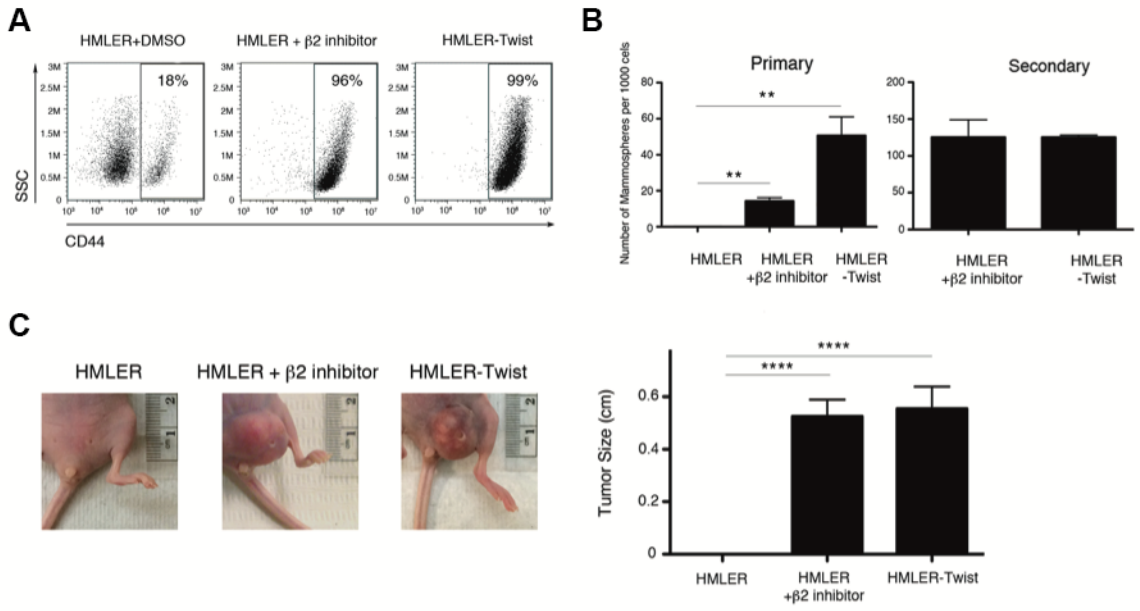

Figure 1.11. Selective inhibition of proteasome activity endows HMLER cells with tumor-initiating capacity in vivo.

(**A)** Flow cytometric analysis of CD44 expression by HMLER-Twist, β2 subunit inhibitor-treated or DMSO-treated HMLER cells. Percentage of $CD44^{high}$ cells within the live population is indicated. Representative result of three independent experiments is shown. (**B)** Quantification of primary and secondary mammospheres formed by HMLER, HMLER+β2 inhibitor, or HMLER-Twist, presented in the bar graph as the number of mammospheres formed per 1000 seeded cells. Error bars indicate SEM ($n \geq 3$). (**C)** Primary tumor formation in immunodeficient mice 2 months after injection with HMLER, HMLER+β2 inhibitor, or HMLER-Twist cells. Error bars indicate SEM ($n = 12$ mice per group). Representative images of the tumors are also shown.

CHAPTER 2: SELECTIVE INHIBITION OF PROTEASOME ACTIVITY INDUCES EMT-ASSOCIATED TRASNCRIPTOME CHANGES BY STABILIZING THE TGF-B RECEPTOR

2.1: Introduction

Because of my observation that proteasome activity is both associated with and regulates EMT phenotypes and functionality, I hypothesized that a decrease in proteasome activity is effectively sparing an unknown factor from degradation that is, in turn, potentiating EMT. In this chapter, I search for potential mechanisms by which low proteasome activity might be inducing EMT by using transcriptome analysis. Further, I show that decreased proteasome activity is causing EMT, in part, by sparing the TGF-β receptor (TGFBR) from degradation, and allowing increased sensitivity to autocrine TGF-β signaling.

2.2: Results

2.2.1: Selective inhibition of proteasome activity induces an EMT transcriptional program

To investigate the molecular mechanisms underlying proteasome inhibitor-induced EMT, I performed gene expression microarray analysis of DMSO-treated HMLE cells, cells treated with either β2 or β5 subunit inhibitors, and cells expressing Snail. 1,338 and 1,278 genes were differentially expressed in β2 and β5 subunit inhibitor-treated HMLE cells, respectively, compared to DMSO-treated cells. Among these differentially expressed genes were a number of transcripts that have been previously reported to be associated with EMT (**Figure 2.1**). These included a number of upregulated mesenchymal markers *ID1*, *KLK7*, *LCN2*, and *CEACAM6* as well as downregulated epithelial markers *FOXA2*, *MIR205*, and *COL4A2* (11). Moreover, key genes were validated by qPCR and I found that β2 and β5 inhibitor-treated HMLE cells exhibited increased expression of the EMT-associated transcription factors, *SNAI1, ZEB1/2*, and *TWIST1*, as well as decreased expression of epithelial markers *CDH1*, *TJP1*, and *CLDN1* (**Figure 2.1**).

Gene set enrichment analysis (GSEA) revealed that transcripts upregulated or downregulated upon proteasome inhibitor treatment were significantly enriched within the set of genes upregulated or downregulated in HMLE-Snail, respectively (**Figure 2.2**). These observations were confirmed by additional GSEA using datasets derived from the Molecular Signatures Database (**Supplementary Table 1**). Lastly, I applied Ingenuity Pathway Analysis (IPA) to the transcripts that were differentially expressed between β2 or β5 subunit inhibitor-treated HMLE cells and DMSO-treated cells. This analysis identified cellular movement, cell death and survival, cell growth and proliferation, and EMT as some of the most significantly enriched molecular and cellular functions across all samples (**Fig. 2.1, Supplementary Table 2**). Taken together, these analyses provide molecular evidence that β2 or β5 subunit inhibition induces HMLE cells to undergo EMT.

2.2.2: Selective proteasome inhibitor enhances TGF-β signaling

In addition to identifying a link between proteasome inhibition and the EMT pathway, IPA analysis also identified the TGF-β1 signaling pathway as a putative upstream regulator driving the observed transcriptional changes in proteasome-inhibited HMLE cells (**Supplementary Table 2, Fig. 2.3**). TGF-β1 signals through tetrameric TGF-β receptors 1 (TGFR1) and 2 (TGFR2) complexes, which phosphorylate SMAD2 (pSMAD2). SMAD4 combines with pSMAD2 to form multimeric SMAD-complexes that translocate into the nucleus and regulate transcription (11). I hypothesized that reduced proteasome activity might result in increased stability of TGFR2 leading to increased TGF-β1 signaling. In support of this hypothesis, I observed increased cell surface expression of TGFR2 in HMLE cells treated with β2 subunit inhibitor (**Fig. 2.3**). Moreover, I found that treatment with β2 subunit inhibitor increased SMAD2 phosphorylation and increased SMAD4 nuclear localization by 2-fold

compared to DMSO-treated cells (**Fig. 2.3**). In line with these results, I also observed increased mRNA expression of SMAD target genes *SNAI1*, *ZEB1*/*2*, *MMP2*, and *MMP9*, as well as decreased expression of *SMAD7*, a negative regulator of TGF-β1 signaling (**Fig. 2.1**).

2.2.3: Proteasome inhibitor-induced EMT is dependent on TGF-β1 signaling

To confirm that EMT induction in proteasome inhibitor-treated HMLE cells is due to TGF-β1 signaling, I repeated inhibitor treatment in the presence of an anti-TGF-β1 neutralizing antibody. I first validated the specificity of the neutralizing antibody in my system by showing that SMAD2 phosphorylation is blocked when HMLE cells are treated with TGF-β1 or proteasome inhibitors in the presence of the neutralizing antibody (**Fig. 2.4**). Strikingly, I found that neutralizing anti-TGF-β1 antibodies prevented the β2 subunit inhibitor-induced increase in CD44 cell surface expression (**Fig. 2.5**). Moreover, EMT-associated downregulation of E-cadherin and upregulation of fibronectin and vimentin, both at the protein and mRNA level, were prevented by anti-TGF-β1 antibody treatment (**Fig. 2.5**). Taken together, these data suggest that a consequence of decreased β2 subunit proteasome activity in HMLE cells is the stabilization of the TGFR2 at the cell surface, thereby resulting in increased TGF-β1 signaling and induction of the EMT transcriptional program.

2.3: Conclusion

Transcriptomic analyses suggested that proteasome-inhibited cells share gene expression signatures with cells that had undergone EMT, in part, through modulation of the TGF-β signaling pathway, a potent inducer of EMT. However, it remains possible that a decrease in proteasome activity may enhance the stability of other EMT-promoting factors. For example, glycogen synthase kinase-3β (GSK3β)-mediated phosphorylation of SNAI1 has been shown to facilitate its nuclear export and degradation (11,45), while SNAI2 can undergo proteasome-

dependent degradation mediated by the p53-MDM2 complex (11,46). In addition, phosphorylation of TWIST1 by the MAPK p38-JNK-ERK complex protects it from degradation (11,47). Thus, downregulation of proteasome activity may lead to the induction of the EMT program through effects mediated by other pathways in addition to enhanced TGF-β1 signaling.

Chapter 2, in full, is an adapted version of material published in *Oncotarget*. Banno, Asoka; Garcia, Daniel A.; van Baarsel, Eric D.; Metz, Patrick J.; Fisch, Kathleen; Widjaja, Christella E.; Kim, Stephanie H.; Lopez, Justine; Chang, Aaron N.; Geurink, Paul P.; Florea, Bogdan I.; Overkleeft, Hermen S.; Ovaa, Huib; Bui, Jack D.; Yang, Jing; Chang, John T.; Downregulation of 26S proteasome catalytic activity promotes epithelial-mesenchymal transition, *Oncotarget*, 2016, 7:21527-21541. The dissertation author was the co-primary author of all material.

Figure 2.1. Selective inhibition of proteasome activity induces an EMT transcriptional program.

(**A**) Volcano plots depicting differentially expressed genes in HMLE cells treated with β2 or β5 subunit inhibitors compared to DMSO-treated cells after 10 days. X-axis represents the Array Studio estimate and the y-axis represents the $-Log_{10}$(Raw P-value). Significant differentially expressed genes are highlighted in red (upregulated) or in blue (downregulated). Selected genes of interest are indicated. (**B)** mRNA levels of epithelial and mesenchymal markers in sorted $CD44^{high}$ HMLE cells treated with β2 (black bars) or β5 inhibitor (grey bars). GAPDH was used as a reference gene. Data are shown as fold change relative to DMSO-treated HMLE. Error bars indicate SEM ($n \geq 3$). (**C**) Heatmaps depicting Log_2 fold change of differentially expressed genes in the EMT pathway in HMLE cells treated with β2 or β5 subunit inhibitors compared to DMSO-treated cells. Gene list was generated with IPA.

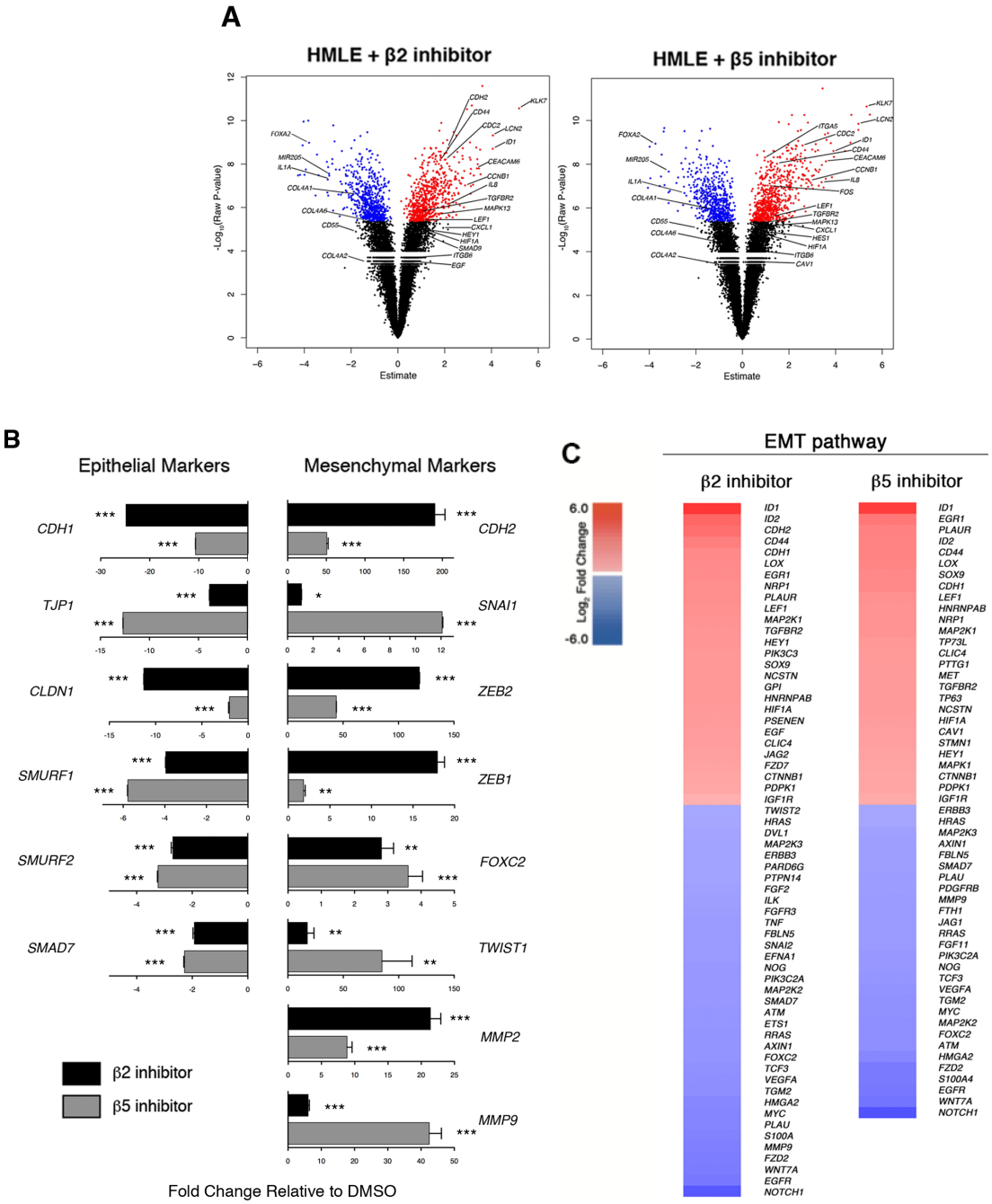
A
HMLE + β2 inhibitor
HMLE + β5 inhibitor
-Log10(Raw P-value)
Estimate
B
Epithelial Markers
Mesenchymal Markers
CDH1
CDH2
TJP1
SNAI1
CLDN1
ZEB2
SMURF1
ZEB1
SMURF2
FOXC2
SMAD7
TWIST1
MMP2
MMP9
β2 inhibitor
β5 inhibitor
Fold Change Relative to DMSO
C
EMT pathway
β2 inhibitor
β5 inhibitor
Log2 Fold Change
6.0
-6.0

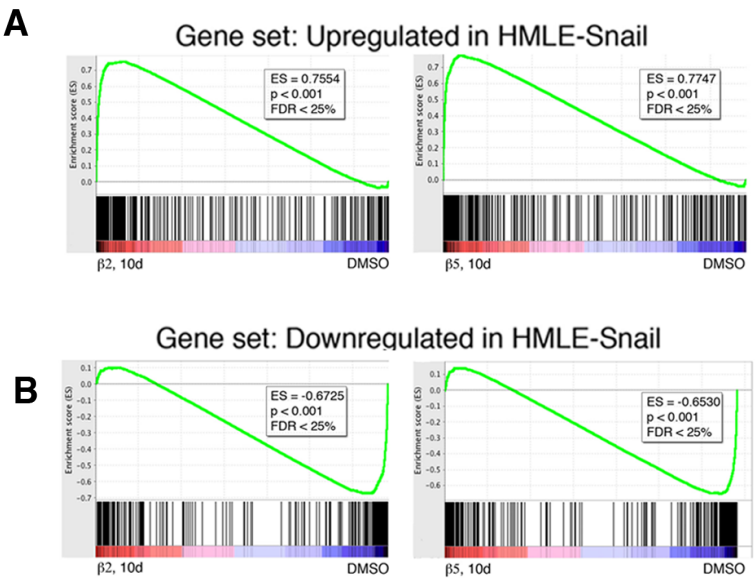

Figure 2.2. Transcriptomes of cells treated with selective proteasome inhibitors are enriched with genes differentially expressed in HMLE-Snail.

(**A, B**) GSEA plots. **(A)** Genes upregulated in HMLE cells treated with β2 or β5 inhibitor are enriched in the set of genes upregulated in HMLE-Snail cells. **(B)** Genes downregulated in HMLE cells treated with β2 or β5 inhibitor are enriched in the set of genes downregulated in HMLE-Snail cells. Enrichment score is visualized in green. ES, enrichment score. FDR, false discovery rate.

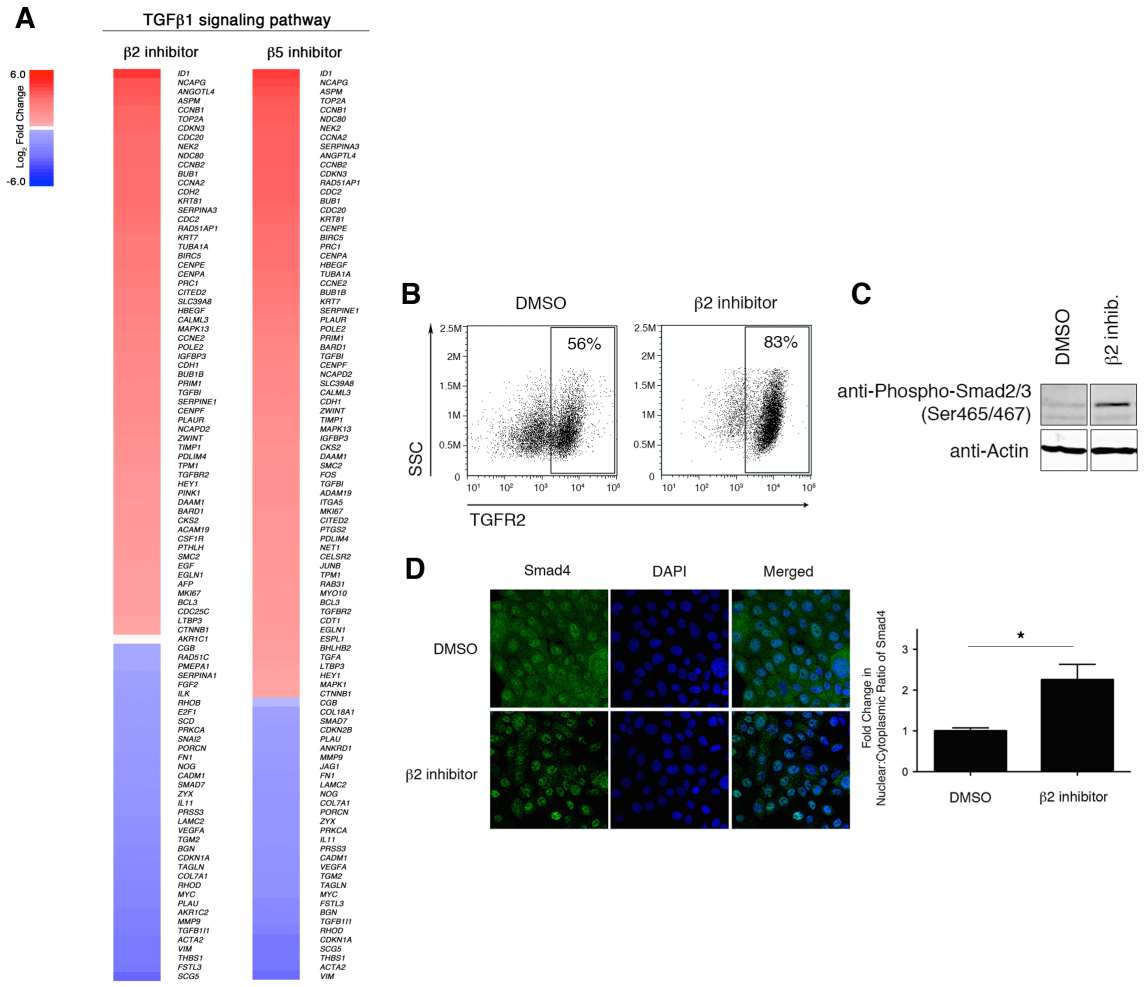

Figure 2.3. Downregulation of proteasome activity enhances TGF-β signaling.
(**A**) Heatmaps depicting Log_2 fold change of differentially expressed genes in the TGF-β1 signaling pathway in HMLE cells treated with β2 or β5 subunit inhibitors compared to DMSO-treated cells. (**B)** Flow cytometric analysis of surface TGFR2 expression and SSC by HMLE cells treated for 1 day with DMSO or β2 subunit inhibitor. Percentage of $TGFR2^+$ cells within the live population is indicated. Representative result of three independent experiments is shown. (**C)** Immunoblot using anti-Phospho-Smad2 (Ser465/467) antibody on whole cell lysates from DMSO- or beta2 inhibitor-treated HMLE cells for 24 hours representative of 3 independent experiments. β-actin served as a loading control. Vertical spaces inserted between lanes indicate removal of intervening, irrelevant samples. All the samples were run on the same gel, transferred and blotted together, and imaged in a single scan. (**D)** Confocal microscopy of Smad4 (green) and DNA (blue; stained with DAPI) in HMLE cells treated with β2 subunit inhibitor for 3 hours. Images were taken at 40X magnification. Bar graph presents fold change in nuclear/cytoplasmic ratio relative to control treatment. Error bars indicate SEM ($n \geq 3$).

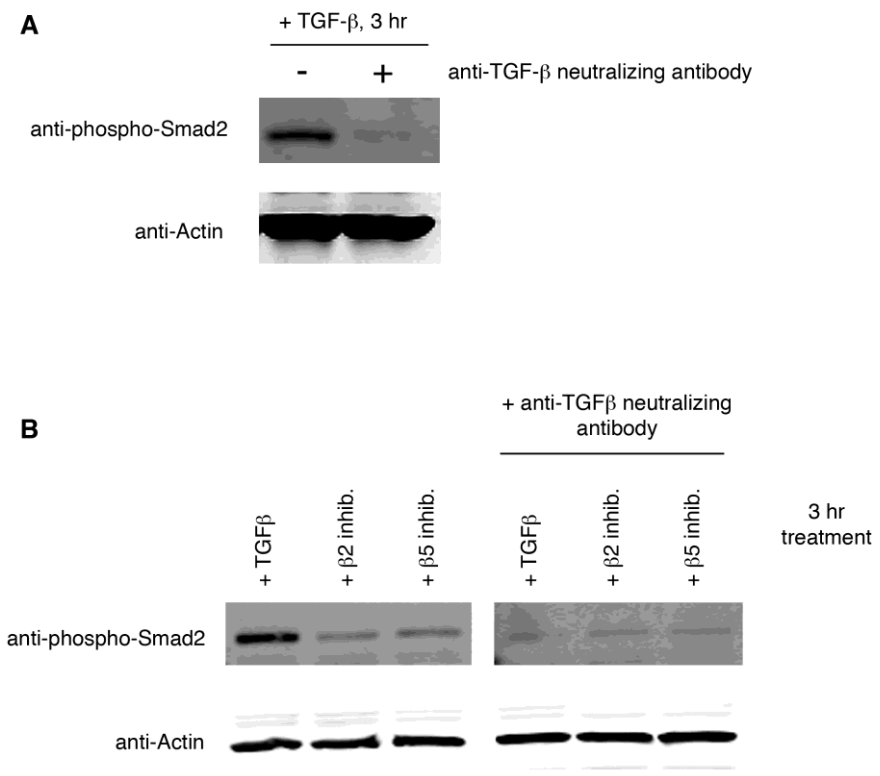

Figure 2.4. Anti-TGF-β neutralizing antibody functions to block TGF-β signaling.
(**A**) Immunoblot of whole cell lysates from HMLE cells treated with 2.5 ng/ml TGF-β for 3 hours with or without 10 μg/ml anti-TGF-β neutralizing antibody. (**B**) Immunoblot of whole cell lysates from HMLE cells treated with 2.5 ng/ml TGF-β or β2 or β5 proteasome subunit inhibitors for 3 hours, with or without 10 μg/ml anti-TGF-β neutralizing antibody.

Figure 2.5. Proteasome inhibitor-induced EMT is dependent on TGF-β signaling.
(**A)** Flow cytometric analysis of CD44 expression after 14 days of treatment with DMSO or β2 inhibitor, with or without neutralizing anti-TGF-β1 antibody. Percentage of $CD44^{high}$ cells within the live population is indicated. Representative result of three independent experiments is shown. (**B)** Confocal microscopy of E-cadherin (left panel; green), fibronectin (right panel; green), or vimentin (red) in HMLE cells, HMLE cells+β2 subunit inhibitor, or HMLE cells+β2 subunit inhibitor with anti-TGF-β1 antibody for 14 days. Images were taken at 40X magnification. (**C)** Immunoblot of whole cell lysates from HMLE, HMLE+β2 inhibitor, or HMLE cells+β2 subunit inhibitor treated with anti-TGF-β1 antibody, using anti-E-cadherin, anti-fibronectin, and anti-vimentin antibodies. Images are representative of 3 independent experiments. β-Actin served as a loading control. Vertical spaces inserted between lanes indicate removal of intervening, irrelevant samples. All the samples were run on the same gel, transferred and blotted together, and imaged in a single scan. (**D)** mRNA levels of epithelial (*CDH1*) and mesenchymal markers (*CDH2*, *ZEB1*, and *VIM*) in HMLE or HMLE+β2 inhibitor treated with or without neutralizing anti-TGF-β1 antibody. GAPDH was used as a reference gene. Data are shown as fold change relative to DMSO-treated HMLE. Error bars indicate SEM ($n \geq 3$).

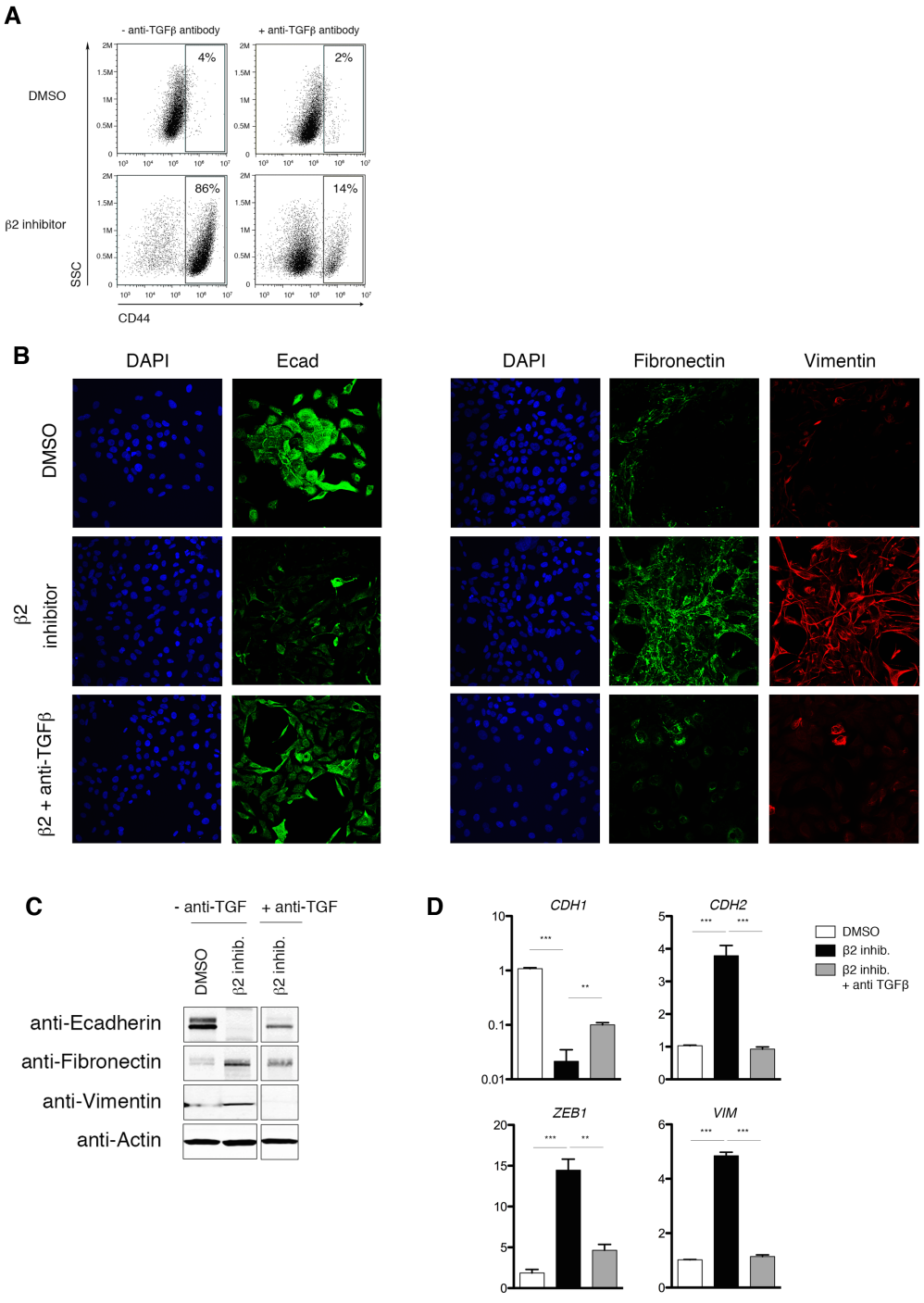
A
- anti-TGFβ antibody
+ anti-TGFβ antibody
DMSO
β2 inhibitor
4%
2%
86%
14%
SSC
CD44
B
DAPI
Ecad
DAPI
Fibronectin
Vimentin
DMSO
β2 inhibitor
β2 + anti-TGFβ
C
- anti-TGF
+ anti-TGF
DMSO
β2 inhib.
β2 inhib.
anti-Ecadherin
anti-Fibronectin
anti-Vimentin
anti-Actin
D
CDH1
CDH2
ZEB1
VIM
DMSO
β2 inhib.
β2 inhib.
+ anti TGFβ

CHAPTER 3: DUB GENE EXPRESSION IS ASSOCIATED WITH EMT

3.1: Introduction

While I have observed that decreased proteasome activity induces EMT and that pharmacological inhibition of proteasome activity can induce EMT, it is still unclear how cells would normally downregulate their proteasome activity during EMT induction. There are a variety of mechanisms by which proteasome activity can be downregulated. For example, individual proteasome subunits can be differentially expressed or modified post-translationally. Alternatively, activity or expression deubiquitinases and ubiquitin ligases can be altered. In search of potential mechanisms, I turned to previously published microarray data to find novel regulators of EMT within the ubiquitin-proteasome pathway.

3.2: Results

3.2.1: DUB expression is associated with EMT

To identify novel regulators of EMT within the ubiquitin-proteasome pathway, I examined previously published microarray data. Taube et al. compared the transcriptomes of immortalized human mammary epithelial (HMLE) cells that have undergone EMT via stable overexpression of EMT-inducing factors (EMT-TFs) Twist, Snail, Gsc, or TGF-β (48). I filtered differentially expressed genes to a curated list of genes within the ubiquitin-proteasome pathway, including the 26S proteasome subunits, ubiquitin ligases, and deubiquitinases. Venn diagram analysis revealed three deubiquitinases – USP11, USP13, and UCHL1 – that were upregulated across all HMLE lines (**Fig. 3.1**). I confirmed the upregulation of DUBs at the protein level (**Fig. 3.1**) in HMLE-Twist and HMLE-Snail compared to the parental line. To show that DUB expression was also differentially expressed without forced overexpression of EMT-TFs, parental HMLE cells were sorted based on their level of cell surface CD44, a previously

established EMT marker (7). In the ~1% of cells that were $CD44^{high}$ within the parental HMLE cell line, DUB expression was markedly increased compared to the rest of the population ($CD44^{low}$) (**Fig. 3.1**). USP11, USP13, and UCHL1 also appear to be a part of the TGF-β-induced EMT pathway, as their expression is upregulated upon TGF-β treatment and EMT induction (**Fig. 3.1**). These results suggest that DUB expression is associated with the EMT, whether cells are induced with TGF-β or stable overexpression of EMT-TFs.

3.2.2: DUB expression is associated with decreased survival in human breast cancer patients

To establish a potential role for DUB expression in human disease progression, I examined their expression in a cohort of breast cancer patients. Using the TCGA invasive breast carcinoma patient dataset, I found that patients with high expression of USP11 and USP13, but not UCHL1, had decreased overall survival compared to patients with low expression (**Fig. 3.2**). Using the web tool Kmplot, I found that only patients with high expression of USP11, not USP13 or UCHL1, exhibited a decreased distant metastasis-free survival (**Fig. 3.2**). These results suggest that DUB expression may contribute to both disease progression and metastasis in human breast cancer patients.

3.2.3: USP11 and its catalytic activity are necessary for a complete acquisition of EMT characteristics in response to TGF-β

To test whether DUBs play a role in regulating EMT, USP11, USP13, and UCHL1 were retrovirally overexpressed in HMLE cells (**Fig. 3.3**). I found that overexpression of these DUBs alone did not cause the cells to undergo EMT. However, when EMT was induced via treatment with TGF-β for 14 days, I observed that cells overexpressing USP11, but not USP13 or UCHL1, exhibited a higher percentage of $CD44^{high}$ cells (**Fig. 3.4**). Based on this result, I decided to focus on the role USP11 plays in regulating TGF-β-induced EMT.

To determine that the effect of USP11 on EMT induction in HMLE cells was due to its deubiquitinating activity, I overexpressed either wild-type USP11 (USP11-wt) or a C318S catalytic mutant of USP11 (USP11-mut) in HMLE cells (**Fig. 3.3**). Unlike USP11-wt, expression of the C318S catalytic mutant failed to enhance EMT, based on CD44 protein expression (**Fig. 3.4**) and mRNA expression of EMT markers *CDH1* (*E-cadherin*), *CDH2* (*N-cadherin*), *VIM*, *ZEB1*, *TWIST1*, and *SNAI1* (**Fig. 3.4**). These results suggest that USP11's deubiquitinating activity is necessary to enhance TGF-β-induced EMT.

I next stably expressed USP11 shRNA in HMLE cells (HMLE-shUSP11) to determine if USP11 is necessary for EMT induction (**Fig. 3.3**). After 14 days of TGF-β treatment, HMLE-shUSP11 cells were unable to undergo EMT to the same extent as cells expressing a non-targeting control shRNA (HMLE-shCtrl). HMLE-shUSP11 cells displayed a significantly lower percentage of $CD44^{high}$ events (**Fig. 3.4**) and failed to upregulate EMT markers to the same extent at HMLE-shCtrl cells (**Fig. 3.4**). Together, these data suggest that while USP11 alone does not induce EMT, it is nonetheless required for TGF-β-induced EMT and is dependent on its catalytic activity to do so.

Cells that have undergone EMT have been shown to possess stem-like characteristics, namely growth in suspension and self-renewal in the mammosphere formation assay (7). I induced EMT with TGF-β treatment for 14 days in the USP11 overexpression and USP11 shRNA HMLE cell lines and then plated them in the mammosphere formation assay (**Fig. 3.5**). I found that overexpression of USP11-wt, but not USP11-mut, increased the number of spheres formed compared to control cells (**Fig. 3.5**), while shRNA knockdown of USP11 reduced the number of spheres formed compared to shCtrl cells (**Fig. 3.5**). This result was expected since the percentage of $CD44^{high}$ cells correlates with the extent of sphere formation. To determine the role

of USP11 in self-renewal, I first sorted cells based on CD44 expression, and then plated them in the sphere assay (**Fig. 3.6**). Neither USP11 overexpression nor USP11 shRNA knockdown affected the number of primary spheres formed when only $CD44^{high}$ cells were plated (**Fig. 3.6**). However, upon serial passage, USP11-wt, but not USP11-mut cells formed more secondary spheres when compared to control cells (**Fig. 3.6**). Conversely, serial passage of shUSP11 spheres resulted in fewer secondary spheres compared to shCtrl (**Fig. 3.6**). These results suggest that USP11 and its deubiquitinating activity are necessary for the self-renewal capacity of human mammary epithelial cells.

3.3: Conclusion

In this study, I show that specific DUBs are upregulated during EMT, and that Ubiquitin specific peptidase 11 (USP11) regulates TGF-β-induced EMT in immortalized human mammary epithelial cells (HMLE), a robust in vitro model for EMT. Overexpression of these DUBs alone does not change their phenotype. However, upon EMT induction with TGF-β, only USP11 overexpression enhanced the EMT phenotype. Further, modulation of USP11 expression affects the development of mesenchymal characteristics in HMLE cells, namely mesenchymal marker expression and self-renewal ability.

These results are in line with previous work that established a role for USP11, but not USP13 or UCHL1, in TGF-β signaling and regulation of TGFBR1 and TGFBR2 stability (49,50). While these studies use mouse or non-mammary cell lines, the current study provides for the first time a thorough phenotypic and functional characterization using a human model of EMT in cells derived from the mammary epithelium.

Further, I correlate increased expression of USP11 with decreased survival in a cohort of breast cancer patients. These findings suggest that USP11 is a novel regulator of TGF-β-induced EMT and could contribute to cancer disease progression in humans. Studies on the role of USP11 in human breast cancer cell lines are addressed in Chapter 4. In addition, USP11's mechanism of action is also explored in Chapter 4.

Chapter 3, in full, is an adapted version of material that has been submitted for publication in *Molecular Cancer Research* and is under review. Garcia, Daniel A.; Baek, Christina; Estrada, M. Valeria; Tysl, Tiffani; Bennett, Eric J.; Yang, Jing; Chang, John T.; *Molecular Cancer Research*, In review. The dissertation author was the primary author of all material.

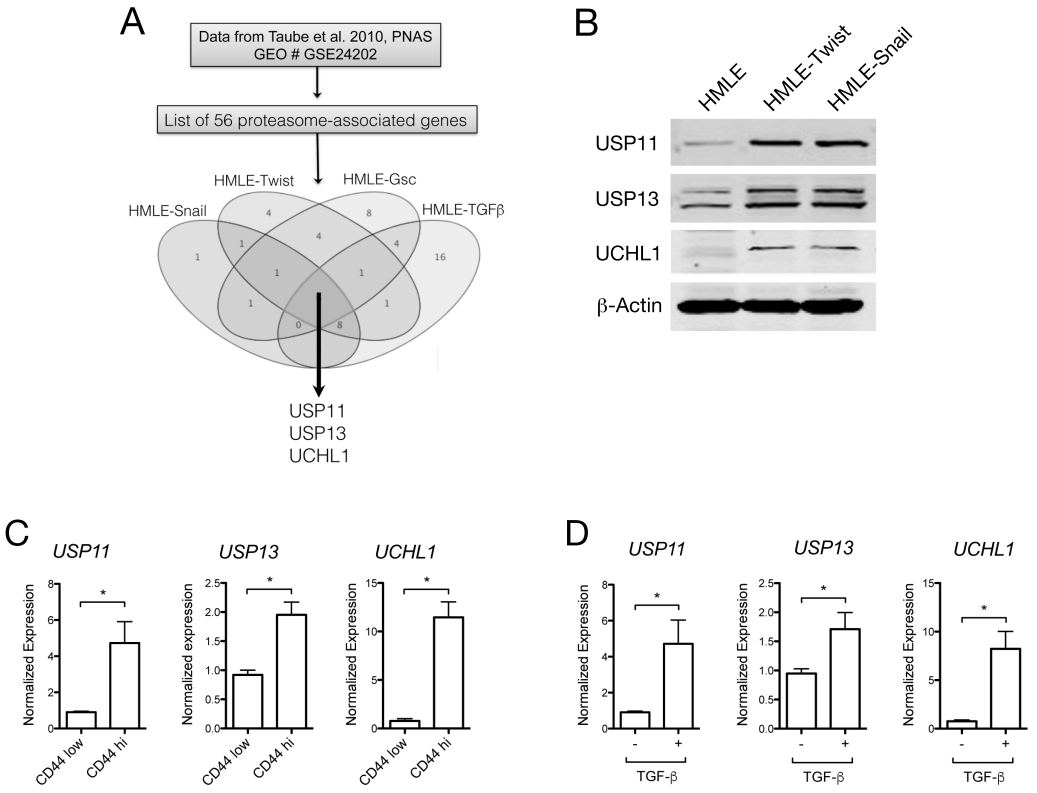

Figure 3.1. DUB expression is associated with EMT.
(**A**) Venn diagram analysis of microarray data from GEO accession GSE24202. Ubiquitin-proteasome system-associated genes were selected from the list of differentially expressed genes. (**B**) Western blot analysis of DUB protein levels in HMLE cells with or without retroviral overexpression of EMT transcription factors. (**C**) qRT-PCR analysis of DUB mRNA levels in HMLE cells sorted based on CD44 cell surface expression level. (**D**) qRT-PCR analysis of DUB mRNA levels in HMLE cells treated or not with TGF-β for 7 days.

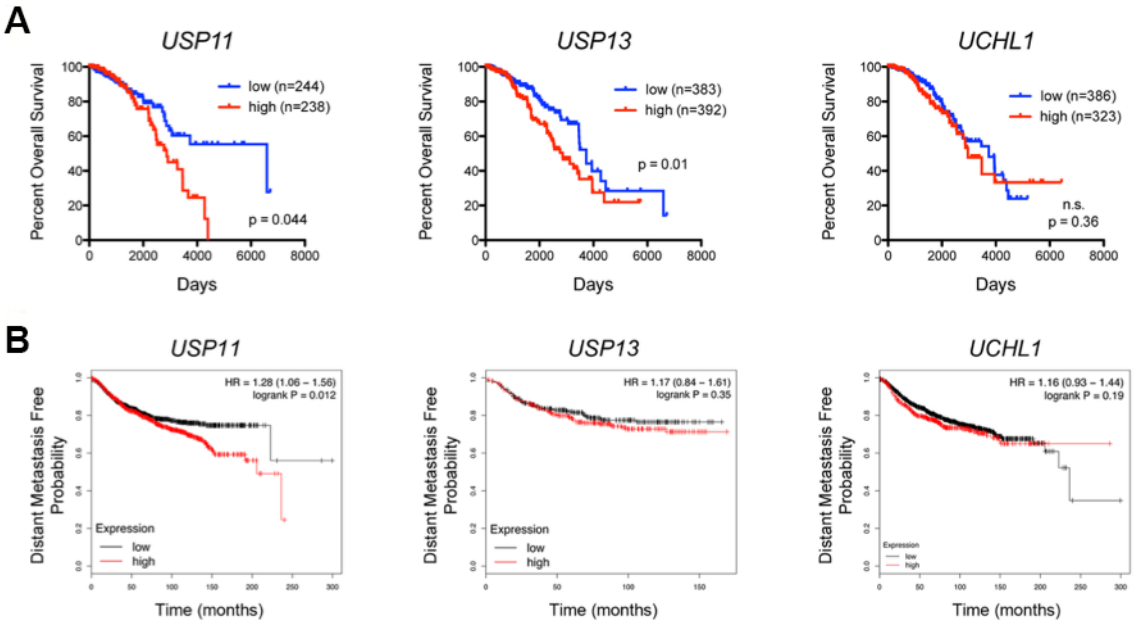

Figure 3.2. DUB expression is associated with decreased survival in human breast cancer patients.

(**A**) Kaplan-Meier analysis of overall survival in relation to the level of DUB gene expression in TCGA breast invasive carcinoma cases. (**B**) Kaplan-Meier analysis of distant metastasis free survival (www.kmplot.com/analysis) in relation to DUB expression in patient tumor samples.

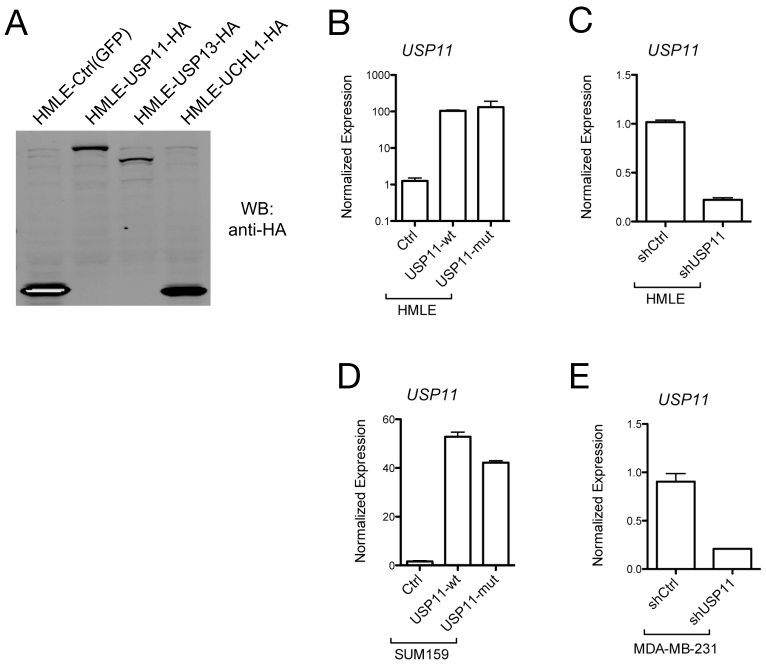

Figure 3.3. Validation of retroviral overexpression and shRNA knockdown of select DUBs. (**A**) Anti-HA western blot analysis of HMLE cells with retroviral overexpression of GFP-HA (Ctrl), USP11-HA, USP13-HA, UCHL1-HA. (**B**) GFP (Ctrl), USP11-wt, and USP11-mut overexpression in HMLE cells at the mRNA level. (**C**) shRNA knockdown of USP11 in HMLE cells at the mRNA level. (**D**) GFP (Ctrl), USP11-wt, and USP11-mut overexpression in SUM159 cells at the mRNA level. (**E**) shRNA knockdown of USP11 in MDA-MB-231 cells at the mRNA level.

Figure 3.4. USP11 and its catalytic activity are necessary for a complete TGF-β-induced EMT.

(**A**, **B**, **D**), Representative flow cytometry analysis of CD44 expression in HMLE cells treated or not with TGF-β for 14 days. (**A**) Retroviral overexpression of DUBs compared to GFP expressing control (Ctrl), (**B**) retroviral overexpression of wild type USP11 (USP11-wt) compared to C318S catalytic mutant USP11 (USP11-mut) and Ctrl, (**D**) retroviral expression of shRNA targeting USP11 (shUSP11) compared to a non-targeting control shRNA (shCtrl). Three independent experiments are represented in the bar graphs. (**C, E**) qPCR analysis of mRNA levels of EMT markers in HMLE cells treated or not with TGF-β for 14 days. (**C**) Retroviral overexpression of wild type USP11 (USP11-wt) compared to C318S catalytic mutant USP11 (USP11-mut) and Ctrl, (**E**) retroviral expression of shRNA targeting USP11 compared to a non-targeting control shRNA (shCtrl). Three independent experiments are represented in the bar graphs.

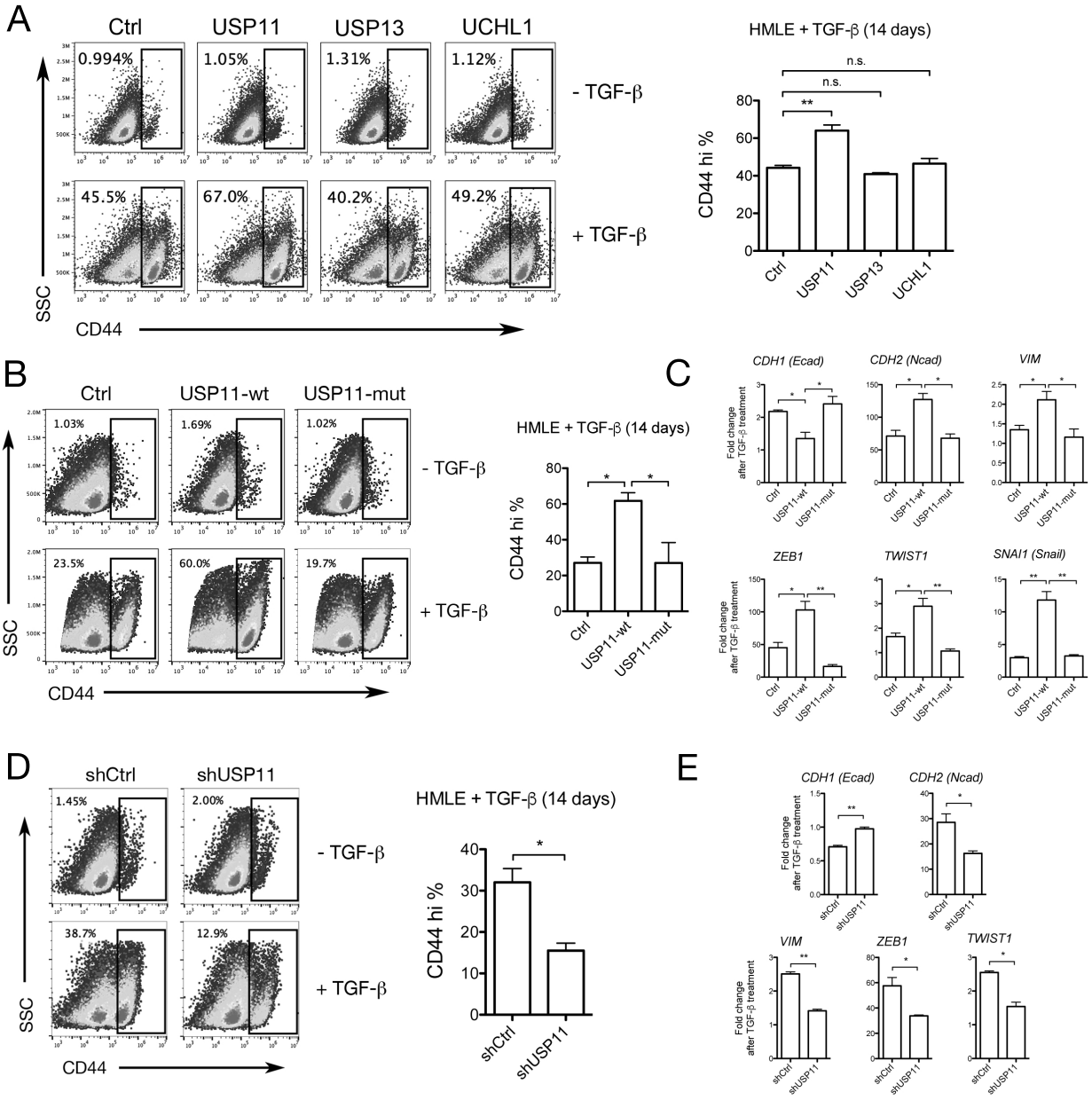
A
Ctrl
USP11
USP13
UCHL1
0.994%
1.05%
1.31%
1.12%
- TGF-β
45.5%
67.0%
40.2%
49.2%
+ TGF-β
SSC
CD44
HMLE + TGF-β (14 days)
n.s.
n.s.
**
CD44 hi %
Ctrl
USP11
USP13
UCHL1
B
Ctrl
USP11-wt
USP11-mut
1.03%
1.69%
1.02%
- TGF-β
23.5%
60.0%
19.7%
+ TGF-β
SSC
CD44
HMLE + TGF-β (14 days)
CD44 hi %
Ctrl
USP11-wt
USP11-mut
C
CDH1 (Ecad)
CDH2 (Ncad)
VIM
ZEB1
TWIST1
SNAI1 (Snail)
Fold change after TGF-β treatment
Ctrl
USP11-wt
USP11-mut
D
shCtrl
shUSP11
1.45%
2.00%
- TGF-β
38.7%
12.9%
+ TGF-β
SSC
CD44
HMLE + TGF-β (14 days)
CD44 hi %
shCtrl
shUSP11
E
CDH1 (Ecad)
CDH2 (Ncad)
VIM
ZEB1
TWIST1
Fold change after TGF-β treatment
shCtrl
shUSP11

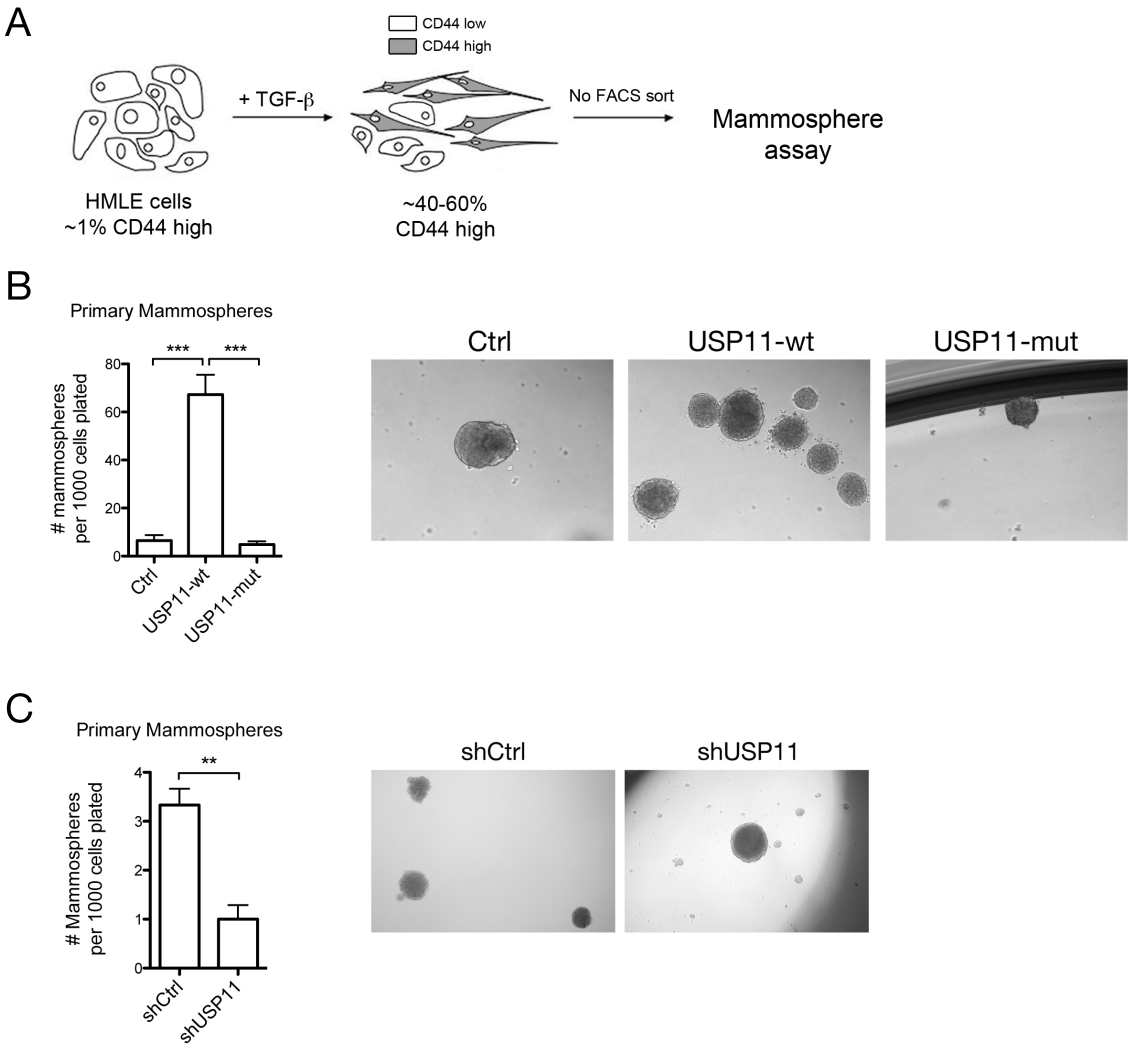

Figure 3.5. USP11 regulates mammosphere formation in normal human epithelial cells. (**A**) HMLE cells were treated with TGF-β for 14 days, then plated directly into the mammosphere assay, without sorting cells. (**B, C**), Primary mammosphere formation of HMLE cells overexpressing either GFP (Ctrl), USP11-wt, or USP11-mut (**B**) or shRNA against USP11 (shUSP11) (**C**) was quantified after 10 days. Three independent experiments are represented in the bar graphs. Representative images of spheres are shown.

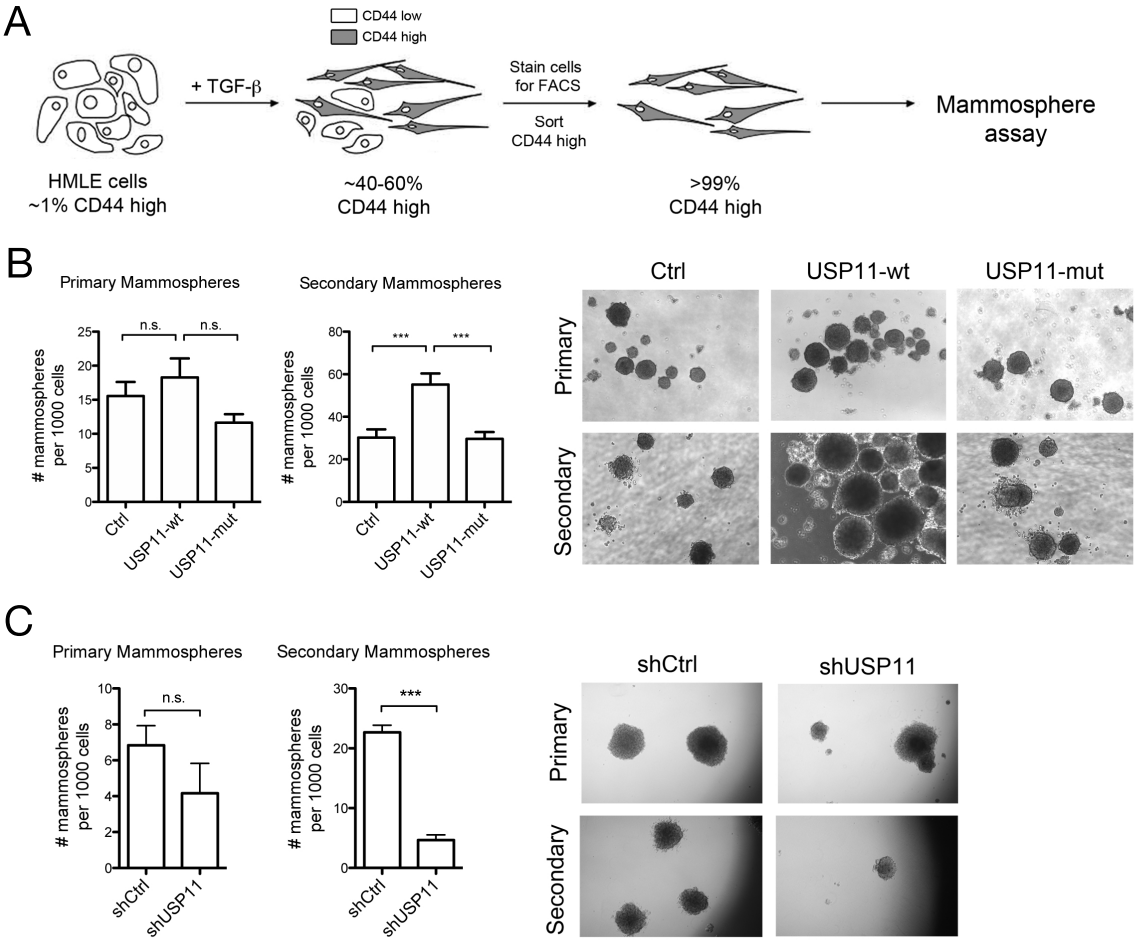

Figure 3.6. USP11 regulates self-renewal in normal human epithelial cells.
(**A**) HMLE cells were treated with TGF-β for 14 days, and then stained for cell surface CD44. $CD44^{high}$ cells were FACS sorted and plated in the mammosphere assay. (**B, C**) Primary mammosphere formation was quantified after 10 days. Primary spheres were dissociated and replated in the secondary mammosphere assay. Secondary sphere formation was quantified after 10 days. Three independent experiments are represented in the bar graphs. Representative images of spheres are shown.

CHAPTER 4: USP11 REGULATES HUMAN BREAST CANCER CELL BEHAVIOR AND METASTASIS

4.1: Introduction

Due to my observation that USP11 regulates normal mammary epithelial cell behavior, I hypothesized that USP11 also regulates human breast cancer cell behavior. In order to study how USP11 affects breast cancer cell behavior, I performed functional experiments in a number of human breast cancer cell lines *in vitro* and *in vivo*. Mechanistically, I show that USP11 affects the stability of TGFBR2 in order to regulate cancer cell behavior and metastasis.

4.2: Results

4.2.1: USP11 is upregulated in human breast cancer cell lines

Since I found that USP11 is upregulated in a panel of human breast cancer cell lines compared to normal mammary epithelial cells (HMLE) (**Fig. 4.1**), I next sought to determine the effects of modulating USP11 expression on the behavior of human breast cancer cells. I chose two human breast cancer cell lines, MDA-MB-231 and SUM159, which exhibited approximately 10-fold and 3-fold upregulation of USP11 compared to HMLE cells (**Fig. 4.1**). In general, I performed shRNA knockdown experiments in MDA-MB-231 cells and retroviral overexpression experiments in SUM159 cells (**Fig. 3.3**). I performed the sphere formation assays in T47D breast cancer cells overexpressing USP11-wt or USP11-mut, or shRNA against USP11, as T47D cells formed the most easily quantifiable spheres in my hands. T47D cells also exhibit upregulated USP11 expression, approximately 20-fold, the highest among the panel of breast cancer cell lines (**Fig. 4.1**), suggesting it may be particularly sensitive to perturbations in USP11 expression.

4.2.2: USP11 and its catalytic activity influence human breast cancer cell migration and self-renewal in vitro

To determine the involvement of USP11 on the *in vitro* behavior of human breast cancer cells, I performed scratch wound and transwell cell migration assays. In a scratch wound closure assay, overexpression of USP11-wt, but not USP11-mut, in SUM159 cells resulted in significantly faster wound closure when compared to control cells (**Fig. 4.2**). USP11 depletion caused MDA-MB-231 cells to close the wound significantly slower when compared to control cells, as evidenced by a significantly larger open area 24 hours after the scratch wound was made (**Fig. 4.2**). The differences seen in wound closure were not due to proliferation, since proliferation was not significantly different across cell lines (**Fig. 4.2**). In a transwell migration assay, overexpression of USP11-wt, but not USP11-mut, caused more SUM159 cells to migrate through the transwell membrane (**Fig. 4.2**). Conversely, shRNA knockdown of USP11 in SUM159 cells caused fewer cells to migrate through the transwell membrane (**Fig. 4.2**). These results suggest that deubiquitination by USP11 regulates collective cell migration in response to a wound (scratch wound assay) and single cell migration in response to a chemoattractant (transwell assay).

In light of my observation that USP11 regulates self-renewal in normal mammary epithelial cells (**Fig. 3.6**), I next sought to determine if USP11 also regulates self-renewal in human breast cancer cells. Neither USP11 overexpression nor shRNA knockdown affected primary sphere formation in T47D human breast cancer cells (**Fig. 4.3**). However, upon serial passage, overexpression of USP11-wt, but not USP11-mut, increased the number of secondary spheres compared to control cells (**Fig. 4.3**). Conversely, USP11 depletion in T47D cells decreased the number of secondary spheres formed compared to shCtrl cells (**Fig. 4.3**). Notably, sphere volume was significantly larger in USP11-wt cells compared to control and USP11-mut cells at the secondary passage, but not the primary passage (**Fig. 4.3**). I also observed smaller

spheres at both primary and secondary sphere passages in T47D cells lacking USP11 compared to shCtrl cells (**Fig. 4.3**). Together, these results show that while USP11 may not affect primary sphere formation, it does regulate secondary sphere formation at subsequent passages suggesting a role in self-renewal. Strikingly, USP11 also affects sphere size, suggesting a role in the proliferative capacity of progenitor cells.

4.2.3: The extent of metastasis of human breast cancer xenografts is dependent on USP11 expression

On the basis of the results from the *in vitro* experiments described above, I hypothesized that modulating USP11 expression in human breast cancer cell lines would affect their behavior *in vivo*. To directly test this hypothesis, I used an experimental tail vein metastasis assay. Indeed, I found that SUM159 cells overexpressing USP11-wt, but not USP11-mut, colonized lung tissue as metastases 10-fold more than control cells (**Fig. 4.4**). Alternatively, when USP11 expression was knocked down with stable shRNA expression, MDA-MB-231 cells colonized lung tissue approximately 40% less than control cells (**Fig. 4.4**). These results suggest that the effect of USP11 expression on *in vitro* behaviors of cancer cell lines can be recapitulated with a more stringent *in vivo* test of metastatic capacity.

4.2.4: USP11 regulates the stability of TGFBR2 and downstream TGF-β signaling in human breast cancer cells

Given the known relationship between TGF-β receptors and DUBs (28,51), specifically USP11 (49,50), I hypothesized that USP11 was affecting TGF-β receptor stability in human breast cancer cells. To determine the mechanism of USP11's effects on cancer cell behavior, I measured the level of TGF-β type II receptor (TGFBR2) using flow cytometry. Overexpression of USP11-wt, but not USP11-mut, caused a 50% increase in TGFBR2 levels in SUM159 cells maintained in normal culture conditions (**Fig. 4.5**). Conversely, USP11 depletion caused a 25%

decrease in TGFBR2 levels in MDA-MB-231 cells maintained in normal culture conditions (**Fig. 4.5**). To investigate the stability and degradation of TGFBR2 in cancer cell lines, I performed a cycloheximide timecourse with simultaneous TGF-β treatment in cells that were serum-starved overnight prior to treatment. While TGFBR2 was degraded over time in all cell lines, TGFBR2 exhibited increased stability in cells overexpressing USP11-wt, but not USP11-mut (**Fig. 4.5**). Conversely, TGFBR2 was degraded more quickly in cells lacking USP11 (**Fig. 4.5**). These results show that USP11 regulates the stability of TGFBR2 during TGF-β stimulation.

To examine how USP11 affects TGF-β signaling, I performed western blots to measure the level of TGF-β pathway activation. I found that USP11 modulates TGF-β signaling over short timescales in human breast cancer cells, as differences in phospho-SMAD2 levels were evident following 30 minutes of TGF-β treatment (**Fig. 4.5**). TGF-β transcriptional activity is also affected by USP11, as the $CAGA_{12}$ SMAD-dependent luciferase reporter (28) was differentially activated when USP11 expression was altered in SUM159 cells (**Fig. 4.5**). Finally, I found that downstream targets of TGF-β are affected by USP11, as USP11 depletion in MDA-MB-231 cells prevented the expression of *PAI-1*, *SNO*, *SKI*, *CTGF*, and *SNAI2* to the same extent as control cells (**Fig. 4.5**). Together, these results confirm that USP11 regulates TGF-β signaling and is essential for TGF-β-dependent responses in human breast cancer cells.

4.3: Conclusion

In this chapter, I show, for the first time in human breast cancer cell lines, that USP11 regulates cell migration, stem-like activity, self-renewal, and metastasis *in vivo*. Specifically, USP11 is necessary and sufficient for proper cell migration as I show in two separate assays – wound closure and transwell migration. In terms of stem-like activity and self-renewal, results varied depending on the passage number of the spheres. While primary sphere formation was not

usually affected, USP11 is clearly necessary and sufficient for secondary sphere formation. Further, USP11 affected the size of the spheres, at both primary and secondary stages. These results suggest that USP11 regulates the self-renewal ability of breast cancer cell lines, which in turn likely impacts their metastatic ability. Notably, I show that USP11 does indeed affect the metastatic ability of two human breast cancer cell lines in an experimental metastasis model. These results suggest that USP11 regulates metastasis by affecting multiple aspects of breast cancer cell behavior, including migration and stem-like characteristics.

To determine USP11's mechanism of action, I investigated different aspects of TGF-β signaling – a pathway known to play an important role in cell migration, invasion, stem-like characteristics, and metastasis. I showed, using multiple different readouts, that USP11 regulates TGF-β signaling. More specifically, I found that USP11 regulates stability of the TGF-β receptor, sparing it from degradation and allowing it to propagate TGF-β signals. These results are in line with previous work that has shown that other DUBs, including USP11, regulate TGFBR1 and TGFBR2. While this relationship has been previously shown in lung fibroblast cells (49), I demonstrate the relevance of this pathway in human breast cancer *in vitro* and *in vivo* models implicating USP11 as a useful therapeutic target in the clinic. It is not outside the realm of possibility that USP11 also deubiquitinates TGFBR1 in human breast cancer cells in order to regulate TGF-β signaling and functional outcomes.

Chapter 4, in full, is an adapted version of material that has been submitted for publication in *Molecular Cancer Research* and is under review. Garcia, Daniel A.; Baek, Christina; Estrada, M. Valeria; Tysl, Tiffani; Bennett, Eric J.; Yang, Jing; Chang, John T.; *Molecular Cancer Research*, In review. The dissertation author was the primary author of all material.

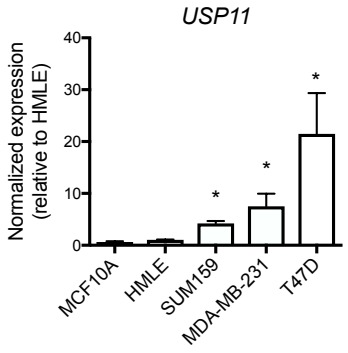

Figure 4.1. USP11 is upregulated in human breast cancer cell lines.
RT-qPCR analysis of USP11 expression in panel of human breast cancer cell lines. Expression was normalized to HMLE levels.

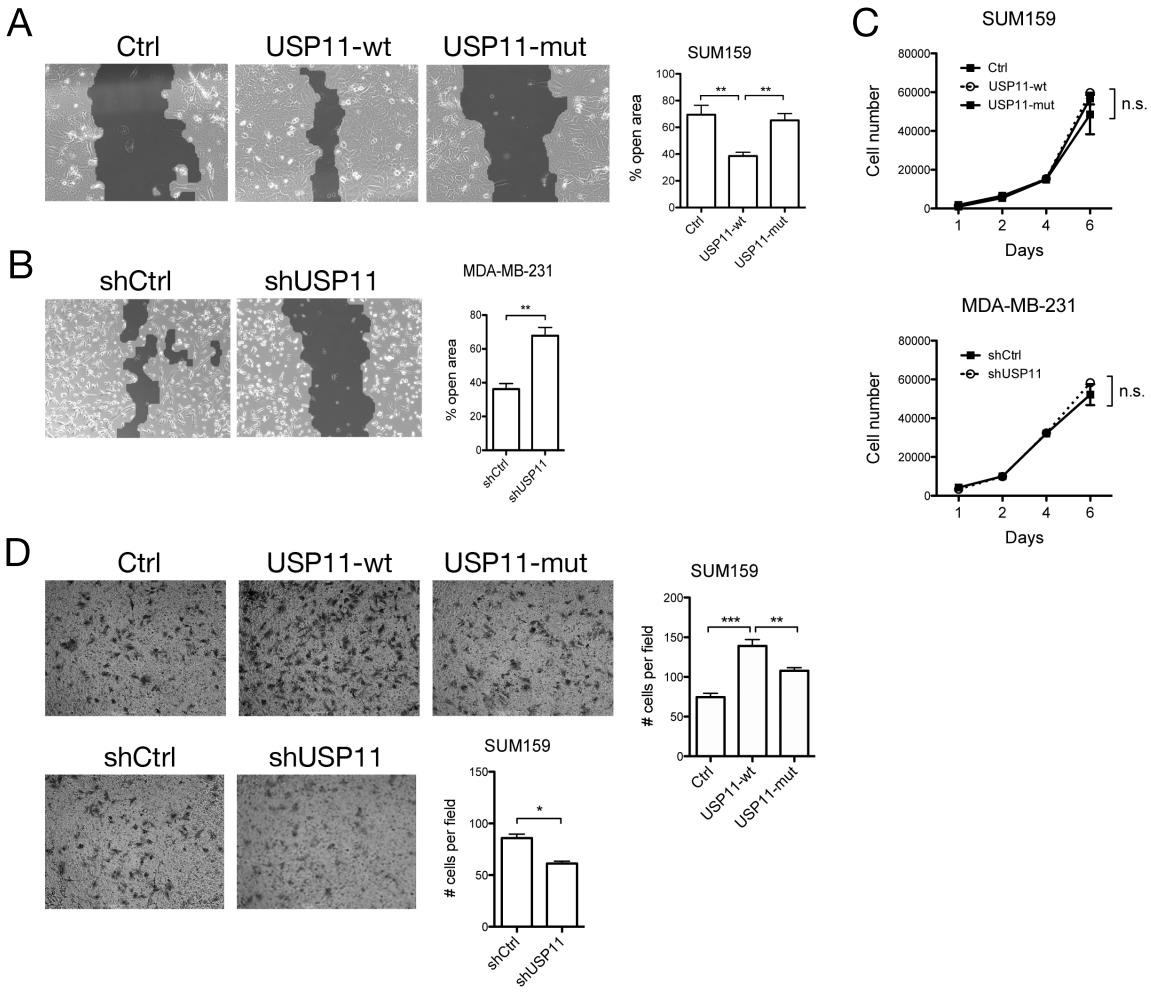

Figure 4.2. USP11 regulates human breast cancer cell migration, but not proliferation. (**A, B**) Scratch wound away was performed with (**A**) SUM159 cells overexpressing GFP (Ctrl), USP11-wt, or USP11-mut and (**B**) MDA-MB-231 cells expressing shCtrl or shUSP11, in media containing TGF-β. Percent open area was quantified by measuring the surface area of the scratch wound at 0 and 24 hours after scratch wound was made. Shown are representative images of the scratch wound 24 hours after scratch was made. Light gray area indicates area covered by cells, while dark gray area indicates the scratch wound. Three independent experiments are represented in the bar graph. (**C**) Cell proliferation assay with SUM159 and MDA-MB-231 cells. (**D**) Transwell migration assay in SUM159 cells. For each experiment, five random microscope fields were photographed and the number of cells per field was quantified using ImageJ. Two independent experiments are represented in the bar graphs.

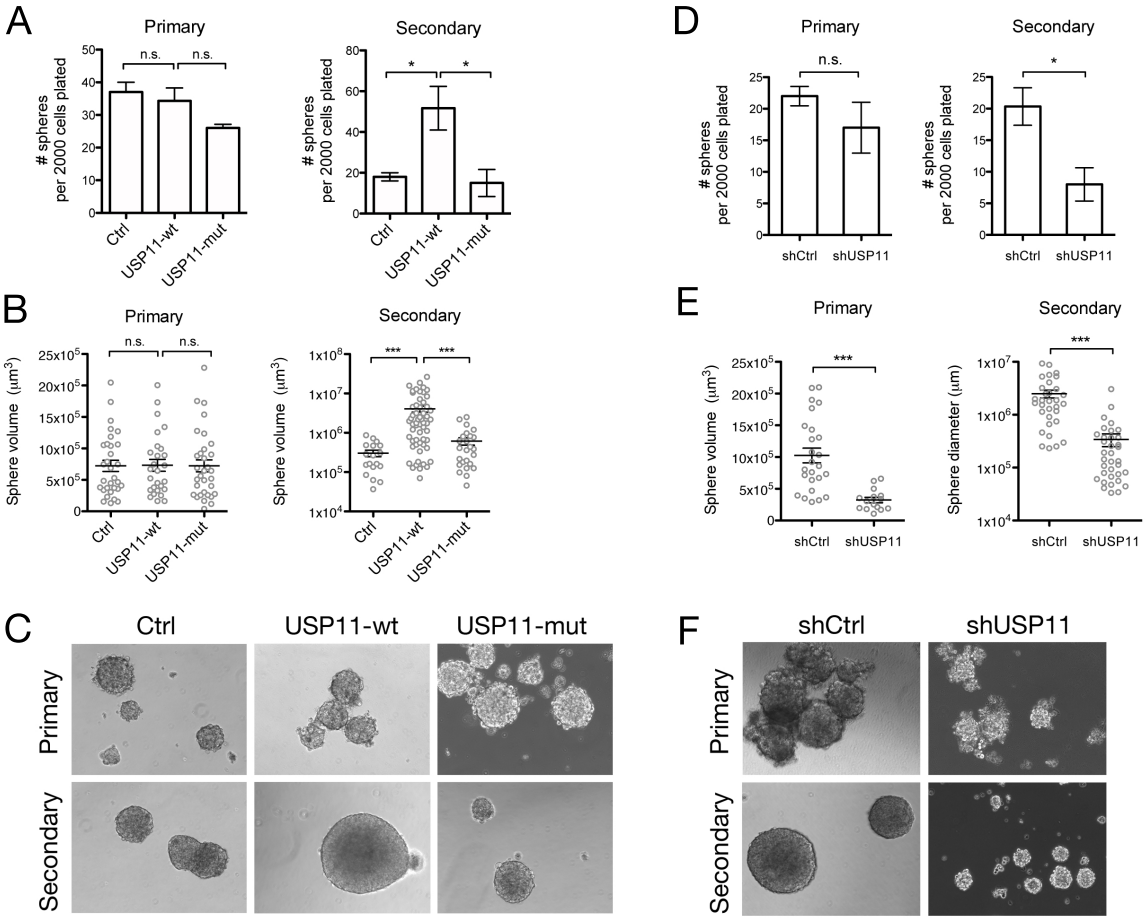

Figure 4.3. USP11 regulates human breast cancer self-renewal.
(**A, B, C**) Primary and secondary sphere formation of T47D cells overexpressing GFP (Ctrl), USP11-wt, or USP11-mut. Sphere number (**A**) and sphere volume (**B**) were quantified. Representative sphere images are shown (**C**). (**D, E, F**) Primary and secondary sphere formation of T47D cells expressing shCtrl or shUSP11. Sphere number (**D**) and sphere volume (**E**) were quantified. Representative sphere images are shown (**F**).

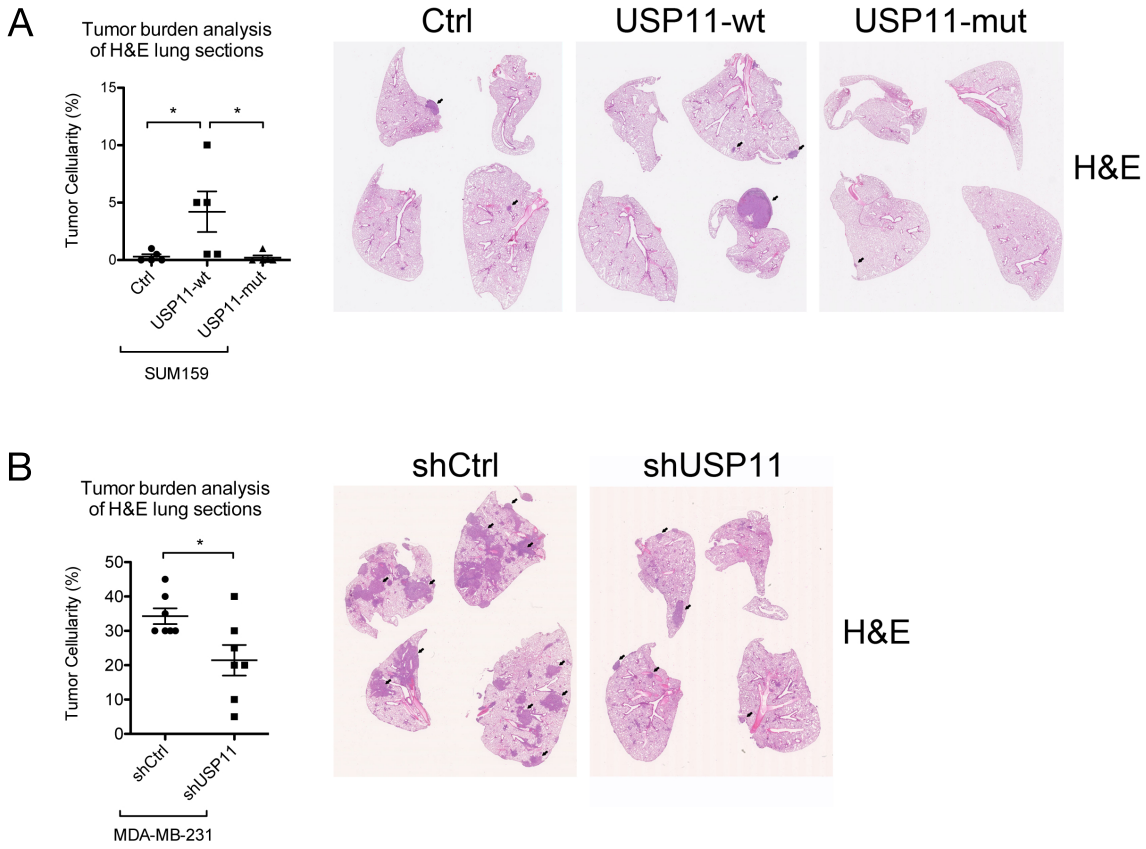

Figure 4.4. USP11 regulates experimental metastasis of human breast cancer cells in mice. Either $1.5x10^6$ SUM159 cells (**A**) or $1x10^6$ MDA-MB-231 cells (**B**) were resuspended in PBS and injected via tail vein into NSG mice at a volume of 100 µl. After 6 weeks, mice were sacrificed and lungs were analyzed for metastatic colonization by fixation, paraffin embedding. H&E-stained sections were examined for percentage of tumor cells amongst normal cells (tumor cellularity). Each data point represents the average tumor cellularity of three step sections (100 um apart) from one mouse. The black arrows indicate examples of metastatic tumors within lung tissue.

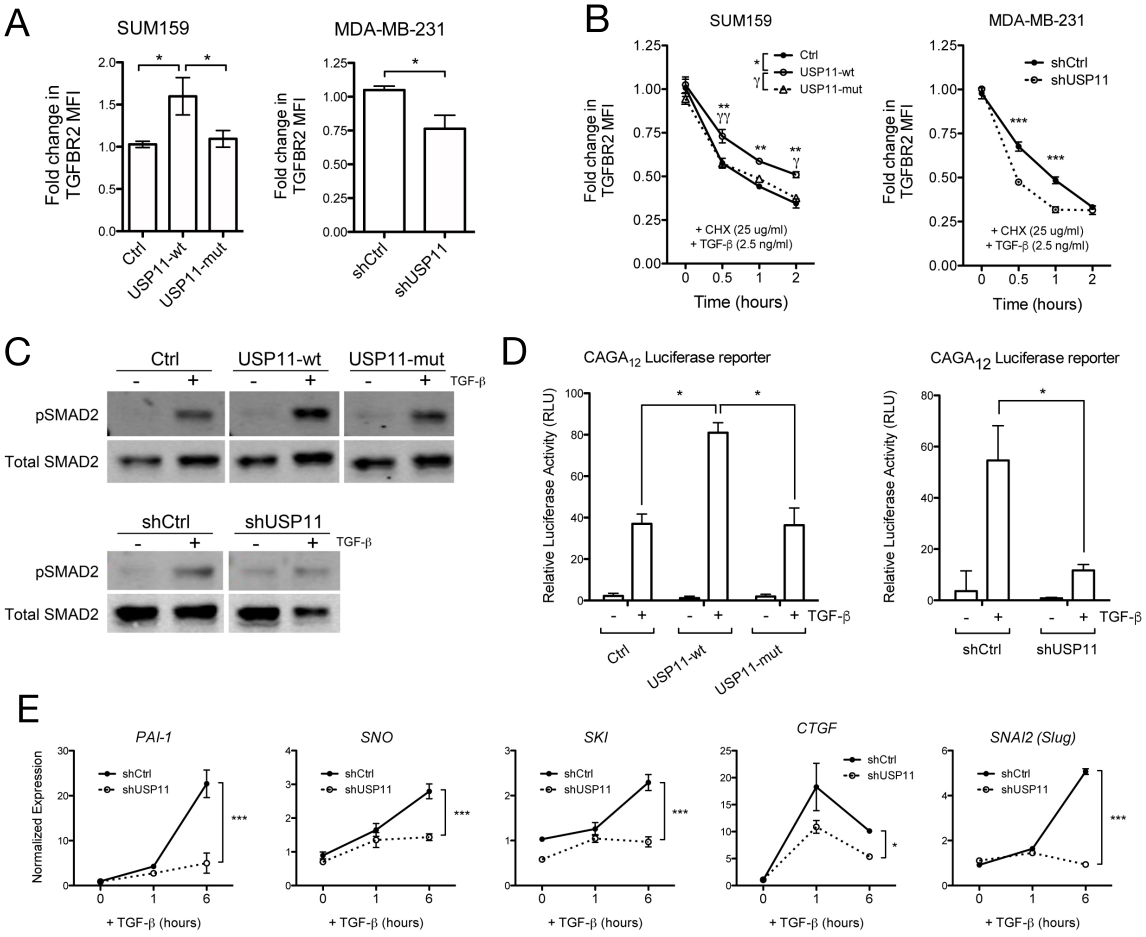

Figure 4.5. USP11 regulates TGFBR2 stability and signaling in human breast cancer cells. (**A**) Flow cytometry analysis of TGFBR2 median fluorescence intensity (MFI) in SUM159 cells overexpressing GFP (Ctrl), USP11-wt, or USP11-mut and MDA-MB-231 cells expressing shCtrl or shUSP11. (**B**) Flow cytometry analysis of TGFBR2 MFI over time after CHX and TGF-β treatment in SUM159 and MDA-MB-231 cells. (**C**) Western blot analysis of phosho-SMAD2 (pSMAD2) in SUM159 cells overexpressing GFP (Ctrl), USP11-wt, or USP11-mut and MDA-MB-231 cells expressing shCtrl or shUSP11 before and after TGF-β treatment for 30 minutes. All blot images are from the same membrane with intervening irrelevant samples not shown. (**D**) Effect of USP11-wt or USP11-mut overexpression and shRNA knockdown on $CAGA_{12}$-luciferase transcriptional response induced by TGF-β in SUM159 cells. (**E**) qRT-PCR analysis of mRNA levels of TGF-β target genes in MDA-MB-231 cells expressing shCtrl or shUSP11.

CHAPTER 5: DISCUSSION

It is established that EMT can generate cells with CSC properties, but the molecular mechanisms that induce and regulate EMT have not been fully elucidated. In the present study, I found that epithelial cells decrease their proteasome activity during EMT and that proteasome inhibitors can induce EMT via stabilization of the TGF-β receptor. Further, I found that deubiquitinase USP11 enhances epithelial-mesenchymal plasticity in both normal and neoplastic mammary cell lines by also stabilizing the TGF-β receptor. These results suggest that the ubiquitin-proteasome system is an important regulator of EMT and could be targeted for use in the clinic to treat or prevent metastasis.

In support of the potential clinical relevance of my observations, I show that proteasome subunit (*PSMB2, PSMB5*) and *USP11* mRNA expression in human tumor samples correlates with disease progression (**Fig. 1.4, Fig. 3.2**). These results are consistent with three previous clinical studies: one study showed that low expression of 19S proteasome subunit *PSMD1* correlates with decreased probability of overall survival in a cohort of 82 head and neck squamous cell carcinoma patients (12); two other studies showed that high *USP11* expression correlates with higher risk of relapse and worse survival outcomes in a cohort of breast cancer patients treated with neoadjuvant therapy (52) and in a cohort of hepatocellular carcinoma patients (53). Conversely, high expression of proteasome subunits *PSMB7* (54) and *PSMB4* (55) has been shown to be associated with decreased breast cancer patient survival and poor prognosis, respectively. The extent to which the expression of *PSMD1*, *PSMB4*, and *PSMB7* affect proteasome activity remains poorly understood, and may provide a possible explanation for these contrasting observations. To my knowledge, this is the first study that suggests a

correlation between decreased expression of the catalytic proteasome subunits - *PSMB2* and *PSMB5* - and reduced survival of breast cancer patients.

My findings are intriguing in light of the clinical use of proteasome inhibitors for the treatment of cancer. While many patients with hematopoietic malignancies respond to the proteasome inhibitor bortezomib, clinical trials investigating the use of proteasome inhibitors for solid tumors, especially breast carcinoma, have thus far been disappointing (1,56-63). One reason for the lack of efficacy of proteasome inhibitors in solid tumors is poor tissue penetrance, but studies have shown that proteasome activity in tumor tissue is decreased in patients that were treated with bortezomib (63). Even ixazomib, a bortezomib analog designed for better tissue penetration, still lacked efficacy in solid tumors (62).

Since tissue penetrance does not seem to be a limiting factor, another potential reason for lack of efficacy of proteasome inhibitors in solid tumors is insufficient potency. Bortezomib, ixazomib, and carfilzomib, all three of which are FDA-approved proteasome inhibitors, primarily target the β5 proteasome subunit, at clinically relevant concentrations. The β1 and β2 subunits have yet to be the subject of targeted pharmaceuticals, even though they also contribute to the overall degradation activity of the 20S proteasome (64). In clinical studies using bortezomib, ixazomib, and carfilzomib, either alone or in combination with conventional therapy, I speculate that inhibiting only β5 subunit activity is insufficient to elicit a response in patients and might even be making the disease progress further. My data suggest a possible molecular mechanism for this observed effect - that pharmacologic inhibition of the proteasome may result in induction of EMT and acquisition of certain attributes of CSCs. Paradoxically, my results also suggest the possibility that pharmacologic inhibition of the proteasome may not only induce EMT in breast cancer cells, but may also endow them with an enhanced capacity to survive against the stimuli

that led to their induction in the first place (**Fig. 1.7**). Taken together, these results suggest caution in the use of proteasome inhibitors in tumor subtypes that follow the CSC paradigm and raise the possibility that the use of agents that activate the proteasome, such as inhibitors of the deubiquitinase USP14 (65), might instead be an effective therapeutic strategy in such cancers.

Yet another reason for the lack of efficacy of proteasome inhibitors in breast cancer is that different breast cancer intrinsic subtypes have different sensitivities to proteasome inhibitors. This is evident in one clinical study that showed, in a cohort of metastatic breast cancer patients treated with bortezomib and doxorubicin, that patients with Basal-like tumors continued to have progressive disease while patients with Luminal A or Luminal B tumors exhibited a partial response or maintained stable disease (61). This could be due to the fact that Basal-like tumors are thought to have undergone EMT, and in their state of decreased proteasome activity, are less sensitive to the effects of proteasome inhibition.

I also found differences in breast cancer prognosis due to USP11 expression when I separate patients based on their intrinsic subtype. High USP11 expression is associated with decreased overall survival and decreased metastasis free survival in patients with Luminal tumor subtype or ER+ tumors, but not Basal-like tumors (**Figure 5.1**). This is likely due to Luminal tumors being more sensitive to EMT stimuli regulated by USP11, namely TGF-β. Since Basal-like tumors have already adopted an EMT phenotype, increased TGF- β signaling via USP11 upregulation is not likely to progress the disease further than it already has. Notably, most ER+ tumors tend to be Luminal-like, further supporting this notion. These analyses show that segregating patients based on tumor subtypes during survival analyses provide additional information to clinicians in terms of what patient populations are more likely to benefit from targeted therapeutics.

While EMT has been studied extensively and clearly plays a role in metastasis, novel druggable regulators of EMT have yet to be uncovered and introduced into the clinic. Since the majority of cancer mortalities are due to metastasis, anti-EMT drugs are an important deficiency in the current arsenal of cancer therapies. In this study, I confirm the role of USP11 in EMT using a robust EMT cell culture model. Furthermore, I establish for the first time USP11's importance in human breast cancer cell migration, self-renewal, and metastasis.

In search of novel regulators of EMT within the ubiquitin-proteasome pathway, I mined previously published microarray data and found USP11, USP13, and UCHL1 to be upregulated during EMT. Using human mammary epithelial cells, a robust in vitro model for EMT, I show that overexpression of these DUBs alone does not change their phenotype. However, upon EMT induction with TGF-β, only USP11 overexpression enhanced the EMT phenotype. Further, modulation of USP11 expression affects the development of mesenchymal characteristics in HMLE cells, namely mesenchymal marker expression and self-renewal ability.

This study is also the first to show the dependence of human breast cancer cells on USP11 for cell migration, self-renewal, and metastasis. I showed that shRNA knockdown of USP11 slowed scratch wound closure and decreased transwell migration, while the opposite effect was shown in a previous study in 786-O cells, a human renal cell adenocarcinoma cell line (66). In that same study, shRNA knockdown of USP11 in 786-O cells also increased cell proliferation, contradicting my result that either overexpression or shRNA knockdown of USP11 in SUM159 and MDA-MB-231 cells, respectively, had no effect on cell proliferation. It is likely that USP11's role is context-specific, having different targets for deubiquitination in different cell types.

In terms of self-renewal, modulating USP11 expression had a significant effect in T47D human breast cancer cells. In general, I found that USP11 is required for proper sphere formation and sufficient to increase sphere formation, specifically at the secondary passage. These results suggest that USP11 is responsible for the maintenance of stem cell characteristics in stem-like human breast cancer cells. Unexpectedly, I observed USP11-dependent effects on sphere size in both T47D cells. Sphere size is not well studied, but it is thought that sphere size indicates the nature of the founder clone cell as being more stem-like in terms of being able to produce more progenitor cells (67). My results show for the first time USP11's role in regulating stem-like behavior of human breast cancer cells in vitro. While sphere number and size are not necessarily a definitive readout of the in vivo presence of cancer stem cells, in vivo models of metastasis are rigorous tests of these characteristics. This study shows that, in this case, the in vivo experimental metastasis model does faithfully recapitulate the in vitro behaviors of human breast cancer cells.

Mechanistically, I show that USP11 enhances TGFBR2 stability, thereby enhancing TGF-β signaling and metastasis (**Fig. 5.2**). USP11 has been shown to target both TGFBR1 and TGFBR2 for deubiquitination (49,50) and my study confirms this pathway for the first time in human breast cancer cells. It is likely that USP11 also deubiquitinates TGFBR1 in human breast cancer cells in order to affect EMT and metastasis. I was unable to study how USP11 affects the stability of TGFBR1 due to the lack of adequate reagents targeting that receptor. However, I suspect that I would find similar results to what I found for TGFBR2.

It has not escaped my notice that other DUBs, namely USP4 and USP15, regulate TGFBR stability (24,28). I speculate that expression of these DUBs likely compensate for the lack of USP11 in cells expressing shRNAs targeting USP11, preventing a complete abrogation or

prevention of the acquisition of EMT phenotypes. It is not surprising that USP4 and USP15 also regulate TGFBR stability, as they are the two most closely related DUBs to USP11 (68,69). I suspect that there remain additional undiscovered layers of regulation of DUB activity that dictate the specificity of USP4, USP15, and USP11 in both time, space, and intensity. It is likely that even minor differences in amino acid sequence and domain structure between related DUBs regulate their intracellular behavior. In fact, USP4 has been shown to be phosphorylated by AKT, thereby regulating its activity (28). It is possible that the activity and subcellular compartmentalization of USP11 and USP15 are regulated in a similar fashion by post-translational modifications.

Furthermore, it is highly likely that USP11 targets many more proteins for deubiquitination that just TGFBR1 and TGFBR2. Using confocal immunofluorescence microscopy, I found that USP11 is localized diffusely in the cytoplasm and intensely in the nucleus (data not shown). This suggests the possibility that USP11 further regulates gene expression in the nucleus by stabilizing transcription factors or epigenetic modulators. Previous work has shown that active proteasomes also reside in the nucleus (70), strengthening the notion that USP11 also function within the nucleus.

Since TGF-β has been linked to EMT and metastasis-promoting functions, it is likely that USP11 regulates the metastatic cascade at multiple points (invasion, intravasation, extravasation, colonization, any step that depends on TGF-β signaling). Thus, my current study establishes the role of USP11 in the complex process of metastasis and suggests USP11 as a potential therapeutic target in breast cancer.

In summary, this dissertation provides and discusses evidence that the ubiquitin-proteasome system is an important regulator of EMT – specifically in terms of both 26S proteasome activity and deubiquitination by USP11. Both of these modes of regulation by the ubiquitin-proteasome system spare protein substrates from being degraded, thereby extending their lifetime and allowing them to perform their function. In both cases, the proteins being spared are likely numerous, but the EMT- and metastasis-promoting proteins dominate, specifically TGFBR2. Importantly, these results contribute to the body of knowledge that suggests that the ubiquitin-proteasome system is essential in regulating both normal and disease states across cell types. Moreover, these results provide a rationale for pursuing the 26S proteasome and USP11 as therapeutic targets for breast cancer.

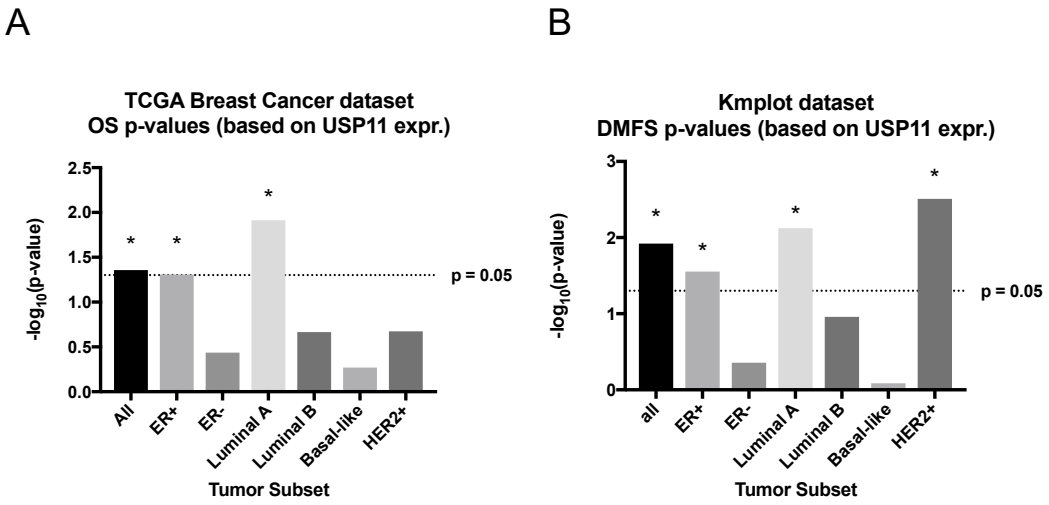

Figure 5.1. Breast cancer patient survival analysis separated by tumor intrinsic subtype. (**A**) P-values of the overall survival (OS) comparison between breast cancer patients with high versus low tumor USP11 expression. Clinical outcome and expression data were sourced from TCGA breast cancer dataset. (**B**) P-values of distant metastasis free survival (DMFS) comparison between breast cancer patients with high versus low tumor USP11 expression. Clinical outcome and expression data were sourced from Kmplot breast cancer dataset.

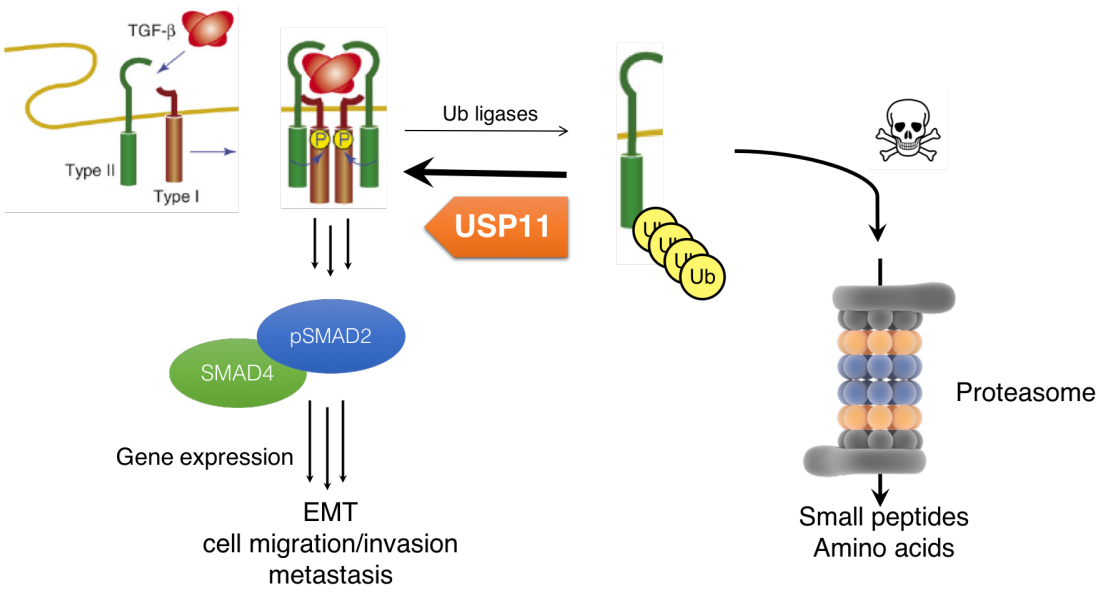

Figure 5.2. USP11 enhances the TGF-β signaling pathway in human breast cancer cells. Extracellular TGF-β binds to its cell surface receptors TGFBR1 and TGFBR2 forming a receptor heterocomplex. Autophosphorylation by the receptor tyrosine kinases initiates the signaling cascade. Phosphorylated SMAD2 (pSMAD2), in complex with SMAD4, is translocated to the nucleus in order to regulate gene expression that leads to EMT and its functional outcomes. Activated TGFBRs are ubiquitinated by ubiquitin ligases and sent to the proteasome for degradation. USP11 removes ubiquitin from the TGFBRs, sparing them from recognition and degradation by the proteasome, and enhancing TGF-β signaling.

APPENDIX A: MATERIALS AND METHODS FOR CHAPTERS 1-2

Animals

All animal work was approved by the Institutional Animal Care and Use Guidelines of the University of California, San Diego. All mice were housed in specific pathogen-free conditions prior to use.

Cell lines

Immortalized human mammary epithelial cells (HMLE), HMLE-Snail, HMLE-Twist, HMLE-Ras (HMLER), and HMLER-Twist were maintained as previously described (34,71). MCF10A cells were obtained from Dr. Karra Muller (UCSD) and cultured in Dulbecco's Modified Eagle's Medium/Nutrient Mixture F-12 supplemented with 5% FBS, 20ng/ml EGF, 0.5mg/ml hydrocortisone, 10μg/ml insulin, 100ng/ml cholera toxin, and penicillin-streptomycin. TGF-β1 treatment was performed as previously reported (7). Epoxomicin (Enzo Life Sciences) was used at 12.5μM. Anti-TGF-β1 neutralizing antibodies (Bio X Cell) were used at a concentration of 10μg/ml.

Activity-based proteasome probes and proteasome inhibitors

Subunit-selective activity-based proteasome probes, MVB003 (pan-reactive), LW124 (β1 subunit-reactive), and PR592 (β5 subunit-reactive) and subunit-selective proteasome inhibitors, NC001 (β1 subunit-reactive), LU102 (β2 subunit-reactive), and LU005 (β5 subunit-reactive) were reconstituted in DMSO and have been previously described (**Figure 1.1**) (36-39). In brief, the proteasome inhibitors were designed for selective and irreversible binding to proteolytically active proteasome subunits. Activity-based probes (ABPs) are similar to the proteasome inhibitors, except that they carry a fluorescent group that allows visualization of proteins bands by SDS-PAGE. For selective proteasome inhibition, cells were cultured in media containing 5% fetal bovine serum in the presence of 5μM β1 inhibitor, 5μM β2 inhibitor, or 0.5μM β5 inhibitor up to 14 days. For analysis of short-term effects of proteasome inhibition on TGF-β signaling, cells were treated for 24 hours.

In-gel proteasome activity assay

Cells were mechanically disrupted in 50mM Tris, pH7.4. 100 μg of total protein was incubated with 0.5μM pan-reactive probe (MVB003), 0.5μM β1 probe (LW124), or 1μM β5 probe (PR592) for 3 hours at 37°C in 50mM Tris, pH7.4 buffer supplemented with 5mM MgCl2, 250mM sucrose, 1mM DTT, and 2mM ATP. After the reaction, samples were resolved on Novex 4-20% Tris-Glycine Mini Protein Gels (Life Technologies) and the fluorescent signals were detected using FluorChem Q (ProteinSimple). Densitometry was used to quantify the

signals. Because the activity-based probes bind stoichiometrically to selective proteasome subunits, the fluorescent signal measured is linearly proportional to the activity of the specific β subunit. Beta2 subunit activity was determined by using the pan-reactive probe (MVB003) and analyzing the fluorescent band at ~23 kiloDaltons.

Immunoblotting and antibodies

Cells were lysed on ice in buffer containing 50mM HEPES, pH7.4, 80mM NaCl, 5mM $MgCl_2$, 10mM EDTA, 5mM sodium pyrophosphate*10 H_2O, 1% TritonX-100, and Protease Inhibitor Cocktail (Sigma-Aldrich). 30 μg of total protein from each sample was resolved on Novex 4-20% Tris-Glycine Mini Protein Gels and transferred onto nitrocellulose membranes. The blots were probed with the appropriate antibodies: anti-ubiquitin (Cell Signaling Technology), anti-β-actin (Sigma-Aldrich), anti-20S/β1 subunit (Santa Cruz Biotechnology, Inc.), anti-20S/β2 subunit (Santa Cruz Biotechnology, Inc.), anti-20S/β5 subunit (Santa Cruz Biotechnology, Inc.), anti-E-cadherin (BD Biosciences), anti-fibronectin (BD Biosciences), anti-vimentin (Cell Signaling Technology), anti-phospho-Smad2 (Ser465/467) (Cell Signaling Technology), or anti-Smad2/3 (Cell Signaling Technology). Signals were detected using Odyssey infrared imaging system (LI-Cor Biosciences).

Flow cytometry analysis and cell sorting

Suspensions of HMLE or MCF10A cells were stained with anti-CD44 antibody (BioLegend), anti-CD24 antibody (BioLegend), 7-AAD (eBioscience), Annexin-V (eBioscience), or anti-TGFR2 antibody (R&D Systems) and analyzed by flow cytometry on a BD Accuri C6 (BD Biosciences). Data were analyzed using FlowJo software. Cell sorting was done using at FACSAria (BD Biosciences) at the UCSD Human Embryonic Stem Cell Core Facility.

Mammosphere culture

Mammosphere culture was performed as previously described (7,72), except that 2,000 single cells for the primary culture and 1,000 dissociated cells for the serial passages were plated per well of a 24-well plate. For serial passage studies, mammospheres were first dissociated into single cells and then plated in mammosphere culture conditions. This process was repeated three times.

Tumorigenesis assay

Five million HMLER cells per group (control HMLER, HMLER-Twist, or HMLER+β2 inhibitor) were injected subcutaneously into homozygous nude mice. A total of 12 animals were used for each condition. The tumor incidence and the tumor size were monitored for two months following injection.

Confocal microscopy

Following growth on coverslips for 2 days and treatment with DMSO, β2 inhibitor, β5 inhibitor or TGF-β1 with or without anti-TGF-β1 antibodies, immunofluorescence of HMLEs and MCF10A was performed as previously described (73) using anti-E-cadherin (BD Biosciences), anti-fibronectin (BD Biosciences), anti-vimentin (Cell Signaling Technology), or anti-Smad4 (B-8) (Santa Cruz Biotechnology) followed by anti-rabbit Alexa Fluor 555 or anti-mouse Alexa Fluor 488 (Life Technologies) antibodies. DAPI (Life Technologies) was used to detect DNA. Acquisition of image stacks was performed as previously described (73) using a FV1000 laser scanning confocal microscope (Olympus). Fluorescence within the nucleus or cytoplasm was quantified using ImageJ software.

Microarray analysis

Total RNA was isolated from HMLE cells using TRIzol (Life Technologies). RNA was extracted from TRIzol using chloroform and precipitated with isopropanol. cDNA was then synthesized using the High Capacity cDNA Reverse Transcription Kit (Life Technologies) and hybridized to HumanHT-12_v4 arrays according to standard protocols (Illumina). Raw data were quantile normalized.

Differential expression analysis of Affymetrix array data was conducted using the Array Studio analysis suite (Omicsoft, Inc). Datasets were quantile-normalized at the gene-level and log-transformed before computing one-way ANOVA statistics between treatment and control group samples. Principal component analysis was used to detect possible outliers and batch effects across samples. Differentially expressed gene signatures representing 1-5% of the coding transcriptomes were generated using a FDR < 0.0001. Functional enrichment of the differentially expressed genes was performed using GSEA, as previously described (74,75), and IPA (Ingenuity). Genes significantly upregulated and downregulated in HMLE-Snail were used as the enrichment set. Other enrichment sets used were taken from the Molecular Signatures Database (75). Enrichment set names are included in Supplementary Table 1.

Real-time quantitative PCR

Total RNA was extracted using TRIzol (Life Technologies) and was reverse-transcribed with MultiScribe Reverse Transcriptase (Life Technologies). The resulting cDNAs were used for qPCR using SsoAdvance SYBR Green Supermix (Bio-Rad) in triplicate. PCR and data collection were performed on CFX96 Touch Real-Time PCR Detection System (Bio-Rad). All the values were normalized to an internal control GAPDH. Relative expression for each target gene was compared to that of HMLE or MCF10A, and the data were presented as relative fold change. See Supplementary Table 3 for primer sequences.

Kaplan-Meier analysis

Kaplan-Meier survival curves were generated from The Cancer Genome Atlas Breast Invasive Carcinoma Illumina HiSeq gene expression dataset (n = 1215). Patients were stratified based on the combined expression of proteasome catalytic subunit genes *PSMB2* and *PSMB5*. High and low expression is defined as the top 20% (n = 245 of 1215) and bottom 22% (n = 277 of 1215) of the patient distribution, respectively. Expression and overall survival data were downloaded from the UCSC Cancer Genomics Browser (https://genome-cancer.ucsc.edu/). Prism (GraphPad) was used to test the statistical significance between the -overall survival curves using the Log-rank (Mantel-Cox) Test.

Oncomine analysis

Oncomine Platform (v4.5, Life Technologies) was used to analyze single gene expression in normal versus tumor samples, using the Finak Breast dataset (44).

Statistics

Statistical analyses were performed with an unpaired *t* test using GraphPad Software. The resulting statistics are indicated in each figure as follows: ns = Not significant ($P > 0.05$), Significant: * = ($P \leq 0.05$), ** = ($P \leq 0.01$), *** = ($P \leq 0.001$), **** = ($P \leq 0.0001$).

APPENDIX B: MATERIALS AND METHODS FOR CHAPTERS 3-4

Animal studies

Animal studies were conducted using procedures approved by the IACUC at the University of California, San Diego (protocol # S09264). Studies were conducted in accordance to the ARRIVE guidelines. NSG mice were obtained from Jackson Laboratories and UCSD Animal Care Program. For the tail vein metastasis assay, SUM159 or MDA-MB-231 cells were resuspended in PBS and injected into the tail vein of 6-8 week old female NSG mice. A total of $1x10^6$-$1.5x10^6$ cells were injected in a volume of 100 μl. Mice were sacrificed after 6-8 weeks and lung metastases were quantified.

Metastasis quantification

Lungs were perfused with PBS and then removed from the thoracic cavity. The lung lobes were fixed in Bouin's solution for 6 hours, and tissue was processed for sectioning and H&E staining. H&E step sections were analyzed by a pathologist (M. V. Estrada) at the Tissue Technology Shared Resource (Moores Cancer Center, UCSD). Tumor burden was assessed by whole section tumor cellularity.

Cell culture

All cell cultures were maintained at 37º C with 5% CO_2. Human mammary epithelial cell lines (HMLE) were cultured in MEGM (Lonza). shRNA and overexpression constructs were retrovirally transduced into HMLE cells. HEK293T, T47D, and MDA-MB-231 cells were cultured in DMEM with 10% FBS. SUM159 cells were cultured in Ham's F12 supplemented with 10 mM HEPES, 5% FBS, 5 μg/ml insulin, and 1 μg/ml hydrocortisone. T47D cells were obtained from Li Ma (University of Texas, MD Anderson Cancer Center). Cell lines were authenticated with ATCC and tested negative for mycoplasma. In general, cells used for experiments were between 2 and 7 passages from thawing.

Vectors

The following retroviral vectors were gifts from Wade Harper: Flag-HA-GFP (Addgene # 22612), Flag-HA-USP13 (Addgene # 22568), Flag-HA-UCHL1 (Addgene # 22563) (76). Full length human USP11 was amplified from a cDNA library and cloned into a retroviral pDEST-Flag-HA vector. Catalytically inactive USP11 was generated by site-directed mutagenesis. shRNA hairpin sequences targeting firefly luciferase or USP11 were cloned into pINDUCER10 (miR-RUP) (77). Stable expression of DUBs and shRNAs was achieved by retroviral infection for 5-7 hours and selection with 2 μg/ml puromycin 24-48 hours later. Retroviruses were produced with HEK293T cells as previously described (22). CAGA12-firefly luciferase reporter

was a gift from Peter ten Dijke (Leiden University Medical Center, Netherlands) (28). pGL4.74-renilla luciferase construct was obtained from Maryan Rizk (Guatelli Lab, University of California, San Diego).

shRNA hairpin sequences

Target: Firefly luciferase (shCtrl) – TGCTGTTGACAGTGAGCGCCCGCCTGAAGTCTCT GATTAATAGTGAAGCCACAGATGTATTAATCAGAGACTTCAGGCGGTTGCCTACTGC CTCGGA

Target: USP11 (shUSP11) – TGCTGTTGACAGTGAGCGACGTGATGATATCTTCGTCT ATTAGTGAAGCCACAGATGTAATAGACGAAGATATCATCACGGTGCCTACTGCCTCG GA

RNA extraction and qRT-PCR

Total RNA was extracted using TRIzol (Thermo-Fisher Scientific) and was reverse-transcribed with High-Capacity cDNA Reverse Transcription Kit (Thermo-Fisher Scientific). The resulting cDNAs were used for qPCR using SsoAdvance SYBR Green Supermix (Bio-Rad) in triplicate. qPCR and data collection were performed on CFX96 Touch Real-Time PCR Detection System (Bio-Rad). All the values were normalized to an internal control GAPDH. Relative expression for each target gene was compared to that of cells expressing Ctrl or shCtrl.

Microarray and Kaplan-Meier analysis

Microarray data from GEO accession GSE24202 (48) were analyzed with IPA (Qiagen). Briefly, 56 genes associated with the ubiquitin-proteasome pathway were chosen from the list of differentially expressed genes as determined by IPA. Venn diagram analysis was performed using the list of 56 genes. Kaplan-Meier survival curves for overall survival were generated from The Cancer Genome Atlas Breast Invasive Carcinoma gene expression dataset (n = 1215). Patients were stratified based on the expression of USP11, USP13, or UCHL1. High and low expression were defined as the top and bottom ~25% of the patient distribution. Expression and overall survival data were downloaded from the UCSC Cancer Genomics Browser (https://genome-cancer.ucsc.edu/). Prism (GraphPad) was used to test the statistical significance between the overall survival curves using the Log-rank (Mantel-Cox) Test. Kaplan-Meier survival curves for distant metastasis free survival were generated with the web tool http://www.kmplot.com/analysis (78).

Flow cytometry analysis

Suspensions of HMLE cell lines were stained with anti-CD44 antibody (BioLegend) and analyzed by flow cytometry on a BD Accuri C6 (BD Biosciences). Suspensions of MDA-MB-

231 and SUM159 cell lines were fixed and permeabilized with the fixation/permeabilization concentrate kit (eBioscience), and stained with anti-TGFBR2 antibody (R&D). Data were analyzed using FlowJo software. Cell sorting was done using a FACS Aria 2 (BD Biosciences) at the UCSD Human Embryonic Stem Cell Core Facility.

Mammosphere assay

HMLE mammosphere culture was performed by plating 1,000-5,000 cells in Mammocult medium (Stemcell Technologies) supplemented with 4 μg/ml heparin, 0.5 μg/ml hydrocortisone, and 1% methylcellulose. For serial passage into secondary mammosphere formation, mammospheres were dissociated into single cells by trypsinization and then plated in mammosphere culture conditions. Spheres were counted 10-12 days later. T47D and SUM159 spheres were formed by plating 1,000-4,000 cells in DMEM/F12 media supplemented with hEGF (20 ng/ml, Sigma), bFGF (20 ng/ml, Thermo-Fisher Scientific), heparin (4 μg/ml, Sigma), 1% methylcellulose (R&D), and B27 Supplement (Thermo-Fisher Scientific). All sphere assays were performed in 24-well ultra low-attachment plates (Corning).

Western blot analysis

Cells were lysed on ice in RIPA buffer supplemented with Protease/Phosphatase Inhibitor Cocktail (Cell Signaling Technology). 30 μg of total protein from each sample was resolved on Novex 4-20% Tris-Glycine Mini Protein Gels and transferred onto nitrocellulose membranes. Blots were probed with the appropriate antibodies: anti-USP11 (Bethyl), anti-USP13 (Bethyl), anti-phospho-SMAD2 (Cell Signaling Technology), anti-total-SMAD2 (Cell Signaling Technology), anti-Flag (eBioscience), anti-HA (eBioscience), or anti-β-actin (Sigma-Aldrich). Signals were detected using fluorescent secondary antibodies compatible with Odyssey infrared imaging system (Li-Cor Biosciences).

Cell migration assays

Scratch wound assays were performed in 6-well plates. Cells were grown to ~90% confluency and wound was created with a pipette tip. Media was replenished with media containing TGF-β (2.5 ng/ml). Images were taken in three separate locations along the scratch wound at 0 and 24 hours after wound was made. Extent of wound closure was analyzed with T-Scratch software. Transwell assays were performed in 24-well polycarbonate inserts (Falcon, 8 μm pore size). Cells were serum starved overnight, then plated in transwell inserts with serum-free media and complete media in the bottom chamber. Cells in the upper part of the transwells were removed with a cotton swab; migrated cells were fixed in 4% paraformaldehyde and stained with crystal violet 0.5%. Three random fields were photographed and the number of cells was counted with ImageJ and averaged. Every experiment was repeated independently at least three times.

Cell proliferation analysis

Cell proliferation was measured using the TetraZ Cell Counting Kit (BioLegend) following manufacturer's instructions.

Dual luciferase reporter assay

SUM159 cell lines were transfected with the TGF-β signaling reporter CAGA12-firefly luciferase and pGL4.74-renilla luciferase (Promega) constructs using Fugene HD (Promega). After 24-48 hours, cells were treated with TGF-β (0.25 ng/ml) for 6 hours. Luciferase activity was then measured using the Dual-Glo Luciferase Assay Kit (Promega).

Statistical analysis

Statistical analyses were performed with an unpaired t test, one-way ANOVA, or two-way ANOVA using GraphPad Software. The resulting statistics are indicated in each figure as follows: ns = not significant ($P > 0.05$), * = ($P \leq 0.05$), ** = ($P \leq 0.01$), *** = ($P \leq 0.001$).

Supplementary Table 1: GSEA with curated gene sets from the Molecular Signatures Database. Gene sets were selected that describe phenotypes and processes related to EMT. β2 and β5 inhibitor-treated HMLE cells are positively enriched in EMT, metastasis, and TGF-β-related gene sets, while negatively enriched in epithelial gene sets. Size indicates the number of genes within Gene Set. NES, Normalized Enrichment Score. Nom., Nominal. FDR, false discovery rate.

			β2 vs DMSO			β5 vs DMSO		
Category	Gene Set Name	Size	NES	Nom. p-value	FDR	NES	Nom. P-value	FDR
Epithelial Characteristics	PROTEINACEOUS_EXTRACELLULAR_MATRIX	98	-1.637	0.002	0.022	-1.723	0.000	0.020
	BASOLATERAL_PLASMA_MEMBRANE	34	-1.615	0.017	0.016	-1.533	0.019	0.030
Epithelial-Mesenchymal Transition	SARRIO_EPITHELIAL_MESENCHYMAL_TRANSITION_UP	165	2.804	0.000	0.000	2.839	0.000	0.000
	ZHANG_BREAST_CANCER_PROGENITORS_UP	233	2.106	0.000	0.000	2.302	0.000	0.000
	ALONSO_METASTASIS_EMT_UP	36	2.073	0.000	0.000	1.868	0.002	0.000
	AIGNER_ZEB1_TARGETS	35	1.655	0.006	0.004	1.714	0.000	0.001
	WANG_TUMOR_INVASIVENESS_UP	244	1.650	0.000	0.003	1.808	0.000	0.000
Metastasis	WINNEPENNINCKX_MELANOMA_METASTASIS_UP	148	2.539	0.000	0.000	2.668	0.000	0.000
	ALONSO_METASTASIS_UP	188	2.199	0.000	0.000	2.111	0.000	0.000
	WANG_METASTASIS_OF_BREAST_CANCER_ESR1_UP	20	1.718	0.004	0.012	1.935	0.000	0.000
	TOMIDA_METASTASIS_UP	26	1.491	0.050	0.094	1.471	0.045	0.036
	CROMER_METASTASIS_UP	75	1.341	0.040	0.118	1.338	0.049	0.078
	RICKMAN_METASTASIS_UP	227	1.203	0.079	0.191	1.153	0.127	0.225
TGFβ	KARAKAS_TGFB1_SIGNALING	18	1.735	0.002	0.007	1.779	0.004	0.013
	COULOUARN_TEMPORAL_TGFB1_SIGNATURE_UP	103	1.578	0.004	0.057	1.752	0.000	0.009
	JAZAG_TGFB1_SIGNALING_UP	104	1.455	0.008	0.107	1.458	0.010	0.092
	RECEPTOR_BINDING	252	1.274	0.033	0.194	1.415	0.008	0.099

Supplementary Table 2: IPA analysis of differentially expressed genes. Transcripts differentially expressed in β2 or β5 inhibitor-treated HMLE cells are enriched in molecular and cellular functions involved in EMT.

		p-value		
Category	**No. of molecules**	**HMLE-Snail**	**HMLE + β2 inhib.**	**HMLE + β5 inhib.**
Cellular Movement	292	6.6×10^{-21}	2.2×10^{-11}	1.4×10^{-11}
Cell Death & Survival	424	4.0×10^{-20}	6.4×10^{-16}	4.3×10^{-15}
Cellular Growth & Proliferation	432	1.6×10^{-18}	7.5×10^{-15}	5.4×10^{-14}
Cell Cycle	233	7.9×10^{-16}	1.5×10^{-10}	2.8×10^{-13}
Epithelial-Mesenchymal Transition	24	4.0×10^{-4}	7.7×10^{-3}	n/a
Cell Cycle: G2/M DNA Damage Checkpoint Regulation	23	5.4×10^{-9}	1.1×10^{-6}	7.0×10^{-7}
TGF-β1 Signaling	99	1.9×10^{-23}	1.2×10^{-20}	1.0×10^{-22}

Supplementary Table 3: Primers for RT-qPCR. All primers are specific for human genes.

Gene	Forward Primer (5' to 3')	Reverse Primer (5' to 3')
CDH1	TGCCCAGAAAATGAAAAAGG	GTGTATGTGGCAATGCGTTC
TJP1	GTCTGCCATTACACGGTCCT	GGTCTCTGCTGGCTTGTTTC
CLDN1	GTGGAGGATTTACTCCTATGCCG	ATCAAGGCACGGGTTGCTT
SMURF1	TGTGAAAAACACATTGGACCCA	ACGCTAATGGTTATCGAATCCG
SMURF2	TATGCAAACTCGGGCCAAATG	CCTGTGCCTATTCGGTCTCTG
SMAD7	GGACGCTGTTGGTACACAAG	GCTGCATAAACTCGTGGTCATTG
CDH2	ACAGTGGCCACCTACAAAGG	CCGAGATGGGGTTGATAATG
SNAI1	CCTCCCTGTCAGATGAGGAC	CCAGGCTGAGGTATTCCTTG
ZEB2	TTCCTGGGCTACGACCATAC	TGTGCTCCATCAAGCAATTC
ZEB1	CCTGTCCATATTGTGATAGAGGC	ACCCAGACTGCGTCACATGT
FOXC2	GCCTAAGGACCTGGTGAAGC	TTGACGAAGCACTCGTTGAG
TWIST1	GGAGTCCGCAGTCTTACGAG	TCTGGAGGACCTGGTAGAGG
MMP2	TGCCTGGAATGCCAT	GTTCTCCAGCTTCAGGTAAT
MMP9	AGCTCATGGGGACTCCTACC	AGACTGCTACCATCCGTCCA
GAPDH	ACCCAGAAGACTGTGGATGG	TCTAGACGGCAGGTCAGGTC
SIP1	TTCCTGGGCTACGACCATAC	TGTGCTCCATCAAGCAATTC
VIM	GAGAACTTTGCCGTTGAAGC	GCTTCCTGTAGGTGGCAATC
FN1	CAGTGGGAGACCTCGAGAAG	TCCCTCGGAACATCAGAAAC
USP11	CATTGAACGCAAGGTCATAGAGC	AACAGTGTGAGATTTGCCCAA
USP13	TCTCCTACGACTCTCCCAATTC	CAGACGCCCCTCTTACCTTCT
UCHL1	GGATTTGAGGATGGATCAGTTC	CCATCCACGTTGTTAAACAGAA
SNAI2	ATGAGGAATCTGGCTGCTGT	CAGGAGAAAATGCCTTTGGA
PAI-1	CACAAATCAGACGGCAGCACT	CATCGGGCGTGGTGAACTC
CTGF	TGCGAAGCTGACCTGGAAGAGAA	AGCTCGGTATGTCTTCATGCTGGT
SKI	AAACTGAATGGGATGGGAGATG	TTTGCATGAATGTCCGTTATCAT
SNO	ATTGCGGCCACGAACTTTTC	GGCTGAACATAAAACTGGGGT

REFERENCES

1. Yang CH, Gonzalez-Angulo AM, Reuben JM, Booser DJ, Pusztai L, Krishnamurthy S, Esseltine D, Stec J, Broglio KR, Islam R, Hortobagyi GN, Cristofanilli M. Bortezomib (VELCADE) in metastatic breast cancer: pharmacodynamics, biological effects, and prediction of clinical benefits. Ann Oncol **2006**;17:813-7

2. Chaffer CL, Weinberg RA. A perspective on cancer cell metastasis. Science **2011**;331:1559-64

3. Weigelt B, Peterse JL, van Veer LJ. Breast cancer metastasis: markers and models. Nature reviews Cancer **2005**;5:591-602

4. Pattabiraman DR, Weinberg RA. Tackling the cancer stem cells - what challenges do they pose? Nat Rev Drug Discov **2014**;13:497-512

5. Chang JT, Mani SA. Sheep, wolf, or werewolf: cancer stem cells and the epithelial-to-mesenchymal transition. Cancer Lett **2013**;341:16-23

6. Hennessy BT, Gonzalez-Angulo AM, Stemke-Hale K, Gilcrease MZ, Krishnamurthy S, Lee JS, Fridlyand J, Sahin A, Agarwal R, Joy C, Liu W, Stivers D, Baggerly K, Carey M, Lluch A, Monteagudo C, He X, Weigman V, Fan C, Palazzo J, Hortobagyi GN, Nolden LK, Wang NJ, Valero V, Gray JW, Perou CM, Mills GB. Characterization of a naturally occurring breast cancer subset enriched in epithelial-to-mesenchymal transition and stem cell characteristics. Cancer Res **2009**;69:4116-24

7. Mani SA, Guo W, Liao MJ, Eaton EN, Ayyanan A, Zhou AY, Brooks M, Reinhard F, Zhang CC, Shipitsin M, Campbell LL, Polyak K, Brisken C, Yang J, Weinberg RA. The epithelial-mesenchymal transition generates cells with properties of stem cells. Cell **2008**;133:704-15

8. Morel AP, Lievre M, Thomas C, Hinkal G, Ansieau S, Puisieux A. Generation of breast cancer stem cells through epithelial-mesenchymal transition. PLoS One **2008**;3:e2888

9. Ouyang G, Wang Z, Fang X, Liu J, Yang CJ. Molecular signaling of the epithelial to mesenchymal transition in generating and maintaining cancer stem cells. Cell Mol Life Sci **2010**;67:2605-18

10. De Craene B, Berx G. Regulatory networks defining EMT during cancer initiation and progression. Nat Rev Cancer **2013**;13:97-110

11. Lamouille S, Xu J, Derynck R. Molecular mechanisms of epithelial-mesenchymal transition. Nat Rev Mol Cell Biol **2014**;15:178-96

12. Lagadec C, Vlashi E, Bhuta S, Lai C, Mischel P, Werner M, Henke M, Pajonk F. Tumor cells with low proteasome subunit expression predict overall survival in head and neck cancer patients. BMC Cancer **2014**;14:152

13. Lagadec C, Vlashi E, Della Donna L, Meng Y, Dekmezian C, Kim K, Pajonk F. Survival and self-renewing capacity of breast cancer initiating cells during fractionated radiation treatment. Breast Cancer Res **2010**;12:R13

14. Pan J, Zhang Q, Wang Y, You M. 26S proteasome activity is down-regulated in lung cancer stem-like cells propagated in vitro. PLoS One **2010**;5:e13298

15. Vlashi E, Kim K, Lagadec C, Donna LD, McDonald JT, Eghbali M, Sayre JW, Stefani E, McBride W, Pajonk F. In vivo imaging, tracking, and targeting of cancer stem cells. J Natl Cancer Inst **2009**;101:350-9

16. Vlashi E, Lagadec C, Chan M, Frohnen P, McDonald AJ, Pajonk F. Targeted elimination of breast cancer cells with low proteasome activity is sufficient for tumor regression. Breast Cancer Res Treat **2013**;141:197-203

17. Adams J. The proteasome: structure, function, and role in the cell. Cancer Treat Rev **2003**;29 Suppl 1:3-9

18. Crawford LJ, Walker B, Irvine AE. Proteasome inhibitors in cancer therapy. J Cell Commun Signal **2011**;5:101-10

19. Bhola NE, Balko JM, Dugger TC, Kuba M, Sánchez V, Sanders M, Stanford J, Cook RS, Arteaga CL. TGF-β inhibition enhances chemotherapy action against triple-negative breast cancer. Journal of Clinical Investigation **2013**;123:1348-58

20. Padua D, Massagué J. Roles of TGFβ in metastasis. Cell Research **2008**;19:89-102

21. Katsuno Y, Lamouille S, Derynck R. TGF-β signaling and epithelial-mesenchymal transition in cancer progression. Current opinion in oncology **2013**;25:76-84

22. Banno A, Garcia DA, van Baarsel ED, Metz PJ, Fisch K, Widjaja CE, Kim SH, Lopez J, Chang AN, Geurink PP, Florea BI, Overkleeft HS, Ovaa H, Bui JD, Yang J, Chang JT. Downregulation of 26S proteasome catalytic activity promotes epithelial-mesenchymal transition. Oncotarget **2016**;7:21527-41

23. Voutsadakis IA. Proteasome expression and activity in cancer and cancer stem cells. Tumor Biology **2017**;39

24. Eichhorn PJA, Rodón L, Gonzàlez-Juncà A, Dirac A, Gili M, Martínez-Sáez E, Aura C, Barba I, Peg V, Prat A, Cuartas I, Jimenez J, García-Dorado D, Sahuquillo J, Bernards R, Baselga J, Seoane J. USP15 stabilizes TGF-β receptor I and promotes oncogenesis through the activation of TGF-β signaling in glioblastoma. Nature Medicine **2012**;18:429-35

25. Wu Y, Wang Y, Lin Y, Liu Y, Wang Y, Jia J, Singh P, Chi Y-II, Wang C, Dong C, Li W, Tao M, Napier D, Shi Q, Deng J, Evers BM, Zhou BP. Dub3 inhibition suppresses breast cancer invasion and metastasis by promoting Snail1 degradation. Nature communications **2017**;8:14228

26. Wu Y, Wang Y, Yang XH, Kang T, Zhao Y, Wang C, Evers BM, Zhou BP. The deubiquitinase USP28 stabilizes LSD1 and confers stem-cell-like traits to breast cancer cells. Cell reports **2013**;5:224-36

27. Zhang J, Zhang P, Wei Y, Piao H-LL, Wang W, Maddika S, Wang M, Chen D, Sun Y, Hung M-CC, Chen J, Ma L. Deubiquitylation and stabilization of PTEN by USP13. Nature cell biology **2013**;15:1486-94

28. Zhang L, Zhou F, Drabsch Y, Gao R, Snaar-Jagalska EB, Mickanin C, Huang H, Sheppard K-A, Porter JA, Lu CX, ten Dijke P. USP4 is regulated by AKT phosphorylation and directly deubiquitylates TGF-β type I receptor. Nature Cell Biology **2012**;14:717-26

29. Zhou Z, Zhang P, Hu X, Kim J, Yao F, Xiao Z, Zeng L, Chang L, Sun Y, Ma L. USP51 promotes deubiquitination and stabilization of ZEB1. American journal of cancer research **2017**;7:2020-31

30. Yang J, Mani SA, Donaher JL, Ramaswamy S, Itzykson RA, Come C, Savagner P, Gitelman I, Richardson A, Weinberg RA. Twist, a master regulator of morphogenesis, plays an essential role in tumor metastasis. Cell **2004**;117:927-39

31. Yang J, Mani SA, Weinberg RA. Exploring a new twist on tumor metastasis. Cancer Res **2006**;66:4549-52

32. Cano A, Perez-Moreno MA, Rodrigo I, Locascio A, Blanco MJ, del Barrio MG, Portillo F, Nieto MA. The transcription factor snail controls epithelial-mesenchymal transitions by repressing E-cadherin expression. Nat Cell Biol **2000**;2:76-83

33. Miettinen PJ, Ebner R, Lopez AR, Derynck R. TGF-beta induced transdifferentiation of mammary epithelial cells to mesenchymal cells: involvement of type I receptors. J Cell Biol **1994**;127:2021-36

34. Elenbaas B, Spirio L, Koerner F, Fleming MD, Zimonjic DB, Donaher JL, Popescu NC, Hahn WC, Weinberg RA. Human breast cancer cells generated by oncogenic transformation of primary mammary epithelial cells. Genes Dev **2001**;15:50-65

35. Berkers CR, van Leeuwen FW, Groothuis TA, Peperzak V, van Tilburg EW, Borst J, Neefjes JJ, Ovaa H. Profiling proteasome activity in tissue with fluorescent probes. Mol Pharm **2007**;4:739-48

36. Li N, Kuo CL, Paniagua G, van den Elst H, Verdoes M, Willems LI, van der Linden WA, Ruben M, van Genderen E, Gubbens J, van Wezel GP, Overkleeft HS, Florea BI. Relative quantification of proteasome activity by activity-based protein profiling and LC-MS/MS. Nat Protoc **2013**;8:1155-68

37. Geurink PP, Liu N, Spaans MP, Downey SL, van den Nieuwendijk AM, van der Marel GA, Kisselev AF, Florea BI, Overkleeft HS. Incorporation of fluorinated phenylalanine

generates highly specific inhibitor of proteasome's chymotrypsin-like sites. J Med Chem **2010**;53:2319-23

38. Britton M, Lucas MM, Downey SL, Screen M, Pletnev AA, Verdoes M, Tokhunts RA, Amir O, Goddard AL, Pelphrey PM, Wright DL, Overkleeft HS, Kisselev AF. Selective inhibitor of proteasome's caspase-like sites sensitizes cells to specific inhibition of chymotrypsin-like sites. Chem Biol **2009**;16:1278-89

39. Geurink PP, van der Linden WA, Mirabella AC, Gallastegui N, de Bruin G, Blom AE, Voges MJ, Mock ED, Florea BI, van der Marel GA, Driessen C, van der Stelt M, Groll M, Overkleeft HS, Kisselev AF. Incorporation of non-natural amino acids improves cell permeability and potency of specific inhibitors of proteasome trypsin-like sites. J Med Chem **2013**;56:1262-75

40. Al-Hajj M, Wicha MS, Benito-Hernandez A, Morrison SJ, Clarke MF. Prospective identification of tumorigenic breast cancer cells. Proc Natl Acad Sci U S A **2003**;100:3983-8

41. Zoller M. CD44: can a cancer-initiating cell profit from an abundantly expressed molecule? Nat Rev Cancer **2011**;11:254-67

42. Moraes RC, Zhang X, Harrington N, Fung JY, Wu MF, Hilsenbeck SG, Allred DC, Lewis MT. Constitutive activation of smoothened (SMO) in mammary glands of transgenic mice leads to increased proliferation, altered differentiation and ductal dysplasia. Development **2007**;134:1231-42

43. Liao MJ, Zhang CC, Zhou B, Zimonjic DB, Mani SA, Kaba M, Gifford A, Reinhardt F, Popescu NC, Guo W, Eaton EN, Lodish HF, Weinberg RA. Enrichment of a population of mammary gland cells that form mammospheres and have in vivo repopulating activity. Cancer Res **2007**;67:8131-8

44. Finak G, Bertos N, Pepin F, Sadekova S, Souleimanova M, Zhao H, Chen H, Omeroglu G, Meterissian S, Omeroglu A, Hallett M, Park M. Stromal gene expression predicts clinical outcome in breast cancer. Nat Med **2008**;14:518-27

45. Zhou BP, Deng J, Xia W, Xu J, Li YM, Gunduz M, Hung MC. Dual regulation of Snail by GSK-3beta-mediated phosphorylation in control of epithelial-mesenchymal transition. Nat Cell Biol **2004**;6:931-40

46. Wang SP, Wang WL, Chang YL, Wu CT, Chao YC, Kao SH, Yuan A, Lin CW, Yang SC, Chan WK, Li KC, Hong TM, Yang PC. p53 controls cancer cell invasion by inducing the MDM2-mediated degradation of Slug. Nat Cell Biol **2009**;11:694-704

47. Hong J, Zhou J, Fu J, He T, Qin J, Wang L, Liao L, Xu J. Phosphorylation of serine 68 of Twist1 by MAPKs stabilizes Twist1 protein and promotes breast cancer cell invasiveness. Cancer Res **2011**;71:3980-90

48. Taube JH, Herschkowitz JI, Komurov K, Zhou AY, Gupta S, Yang J, Hartwell K, Onder TT, Gupta PB, Evans KW, Hollier BG, Ram PT, Lander ES, Rosen JM, Weinberg RA, Mani SA. Core epithelial-to-mesenchymal transition interactome gene-expression signature is associated with claudin-low and metaplastic breast cancer subtypes. Proceedings of the National Academy of Sciences of the United States of America **2010**;107:15449-54

49. Jacko AM, Nan L, Li S, Tan J, Zhao J, Kass DJ, Zhao Y. De-ubiquitinating enzyme, USP11, promotes transforming growth factor β-1 signaling through stabilization of transforming growth factor β receptor II. Cell death & disease **2016**;7

50. Al-Salihi MA, Herhaus L, Macartney T, Sapkota GP. USP11 augments TGFβ signalling by deubiquitylating ALK5. Open biology **2012**;2:120063

51. Aggarwal K, Massagué J. Ubiquitin removal in the TGF-β pathway. Nature Cell Biology **2012**;14:656-7

52. Bayraktar S, Gutierrez Barrera AM, Liu D, Pusztai L, Litton J, Valero V, Hunt K, Hortobagyi GN, Wu Y, Symmans F, Arun B. USP-11 as a predictive and prognostic factor following neoadjuvant therapy in women with breast cancer. Cancer J **2013**;19:10-7

53. Zhang S, Xie C, Li H, Zhang K, Li J, Wang X, Yin Z. Ubiquitin-specific protease 11 serves as a marker of poor prognosis and promotes metastasis in hepatocellular carcinoma. Lab Invest **2018**

54. Munkacsy G, Abdul-Ghani R, Mihaly Z, Tegze B, Tchernitsa O, Surowiak P, Schafer R, Gyorffy B. PSMB7 is associated with anthracycline resistance and is a prognostic biomarker in breast cancer. Br J Cancer **2010**;102:361-8

55. Lee GY, Haverty PM, Li L, Kljavin NM, Bourgon R, Lee J, Stern H, Modrusan Z, Seshagiri S, Zhang Z, Davis D, Stokoe D, Settleman J, de Sauvage FJ, Neve RM. Comparative oncogenomics identifies PSMB4 and SHMT2 as potential cancer driver genes. Cancer Res **2014**;74:3114-26

56. Aghajanian C, Blessing JA, Darcy KM, Reid G, DeGeest K, Rubin SC, Mannel RS, Rotmensch J, Schilder RJ, Riordan W, Gynecologic Oncology G. A phase II evaluation of bortezomib in the treatment of recurrent platinum-sensitive ovarian or primary peritoneal cancer: a Gynecologic Oncology Group study. Gynecol Oncol **2009**;115:215-20

57. Engel RH, Brown JA, Von Roenn JH, O'Regan RM, Bergan R, Badve S, Rademaker A, Gradishar WJ. A phase II study of single agent bortezomib in patients with metastatic breast cancer: a single institution experience. Cancer Invest **2007**;25:733-7

58. Rosenberg JE, Halabi S, Sanford BL, Himelstein AL, Atkins JN, Hohl RJ, Millard F, Bajorin DF, Small EJ, Cancer, Leukemia Group B. Phase II study of bortezomib in

patients with previously treated advanced urothelial tract transitional cell carcinoma: CALGB 90207. Ann Oncol **2008**;19:946-50

59. Awada A, Albanell J, Canney PA, Dirix LY, Gil T, Cardoso F, Gascon P, Piccart MJ, Baselga J. Bortezomib/docetaxel combination therapy in patients with anthracycline-pretreated advanced/metastatic breast cancer: a phase I/II dose-escalation study. Br J Cancer **2008**;98:1500-7

60. Dou QP, Zonder JA. Overview of proteasome inhibitor-based anti-cancer therapies: perspective on bortezomib and second generation proteasome inhibitors versus future generation inhibitors of ubiquitin-proteasome system. Curr Cancer Drug Targets **2014**;14:517-36

61. Irvin WJ, Jr., Orlowski RZ, Chiu WK, Carey LA, Collichio FA, Bernard PS, Stijleman IJ, Perou C, Ivanova A, Dees EC. Phase II study of bortezomib and pegylated liposomal doxorubicin in the treatment of metastatic breast cancer. Clin Breast Cancer **2010**;10:465-70

62. Smith DC, Kalebic T, Infante JR, Siu LL, Sullivan D, Vlahovic G, Kauh JS, Gao F, Berger AJ, Tirrell S, Gupta N, Di Bacco A, Berg D, Liu G, Lin J, Hui AM, Thompson JA. Phase 1 study of ixazomib, an investigational proteasome inhibitor, in advanced non-hematologic malignancies. Invest New Drugs **2015**;33:652-63

63. Trinh XB, Sas L, Van Laere SJ, Prove A, Deleu I, Rasschaert M, Van de Velde H, Vinken P, Vermeulen PB, Van Dam PA, Wojtasik A, De Mesmaeker P, Tjalma WA, Dirix LY. A phase II study of the combination of endocrine treatment and bortezomib in patients with endocrine-resistant metastatic breast cancer. Oncol Rep **2012**;27:657-63

64. Weyburne ES, Wilkins OM, Sha Z, Williams DA, Pletnev AA, de Bruin G, Overkleeft HS, Goldberg AL, Cole MD, Kisselev AF. Inhibition of the Proteasome beta2 Site Sensitizes Triple-Negative Breast Cancer Cells to beta5 Inhibitors and Suppresses Nrf1 Activation. Cell Chem Biol **2017**;24:218-30

65. Lee BH, Lee MJ, Park S, Oh DC, Elsasser S, Chen PC, Gartner C, Dimova N, Hanna J, Gygi SP, Wilson SM, King RW, Finley D. Enhancement of proteasome activity by a small-molecule inhibitor of USP14. Nature **2010**;467:179-84

66. Zhang E, Shen B, Mu X, Qin Y, Zhang F, Liu Y, Xiao J, Zhang P, Wang C, Tan M, Fan Y. Ubiquitin-specific protease 11 (USP11) functions as a tumor suppressor through deubiquitinating and stabilizing VGLL4 protein. American journal of cancer research **2016**;6:2901-9

67. Pastrana E, Silva-Vargas V, Doetsch F. Eyes wide open: a critical review of sphere-formation as an assay for stem cells. Cell stem cell **2011**;8:486-98

68. Harper S, Gratton HE, Cornaciu I, Oberer M, Scott DJ, Emsley J, Dreveny I. Structure and catalytic regulatory function of ubiquitin specific protease 11 N-terminal and ubiquitin-like domains. Biochemistry **2014**;53:2966-78

69. Komander D, Clague MJ, Urbe S. Breaking the chains: structure and function of the deubiquitinases. Nat Rev Mol Cell Biol **2009**;10:550-63

70. von Mikecz A. The nuclear ubiquitin-proteasome system. J Cell Sci **2006**;119:1977-84

71. Tam WL, Lu H, Buikhuisen J, Soh BS, Lim E, Reinhardt F, Wu ZJ, Krall JA, Bierie B, Guo W, Chen X, Liu XS, Brown M, Lim B, Weinberg RA. Protein kinase C alpha is a central signaling node and therapeutic target for breast cancer stem cells. Cancer Cell **2013**;24:347-64

72. Dontu G, Abdallah WM, Foley JM, Jackson KW, Clarke MF, Kawamura MJ, Wicha MS. In vitro propagation and transcriptional profiling of human mammary stem/progenitor cells. Genes Dev **2003**;17:1253-70

73. Chang JT, Palanivel VR, Kinjyo I, Schambach F, Intlekofer AM, Banerjee A, Longworth SA, Vinup KE, Mrass P, Oliaro J, Killeen N, Orange JS, Russell SM, Weninger W, Reiner SL. Asymmetric T lymphocyte division in the initiation of adaptive immune responses. Science **2007**;315:1687-91

74. Mootha VK, Lindgren CM, Eriksson KF, Subramanian A, Sihag S, Lehar J, Puigserver P, Carlsson E, Ridderstrale M, Laurila E, Houstis N, Daly MJ, Patterson N, Mesirov JP, Golub TR, Tamayo P, Spiegelman B, Lander ES, Hirschhorn JN, Altshuler D, Groop LC. PGC-1alpha-responsive genes involved in oxidative phosphorylation are coordinately downregulated in human diabetes. Nat Genet **2003**;34:267-73

75. Subramanian A, Tamayo P, Mootha VK, Mukherjee S, Ebert BL, Gillette MA, Paulovich A, Pomeroy SL, Golub TR, Lander ES, Mesirov JP. Gene set enrichment analysis: a knowledge-based approach for interpreting genome-wide expression profiles. Proc Natl Acad Sci U S A **2005**;102:15545-50

76. Sowa ME, Bennett EJ, Gygi SP, Harper JW. Defining the human deubiquitinating enzyme interaction landscape. Cell **2009**;138:389-403

77. Meerbrey KL, Hu G, Kessler JD, Roarty K, Li MZ, Fang JE, Herschkowitz JI, Burrows AE, Ciccia A, Sun T, Schmitt EM, Bernardi RJ, Fu X, Bland CS, Cooper TA, Schiff R, Rosen JM, Westbrook TF, Elledge SJ. The pINDUCER lentiviral toolkit for inducible RNA interference in vitro and in vivo. Proceedings of the National Academy of Sciences of the United States of America **2011**;108:3665-70

78. Györffy B, Lanczky A, Eklund AC, Denkert C, Budczies J, Li Q, Szallasi Z. An online survival analysis tool to rapidly assess the effect of 22,277 genes on breast cancer prognosis using microarray data of 1,809 patients. Breast Cancer Research and Treatment **2010**;123:725-31